16R-HETE and 16S-HETE Alter Human Cytochrome P450 1B1 through Transcriptional and Allosteric Mechanism

by

Rahmat Hidayat

A thesis submitted in partial fulfilment of the requirements for the degree of

Master of Science

in

Pharmaceutical Sciences

Faculty of Pharmacy and Pharmaceutical Sciences

University of Alberta

Abstract

Cardiac hypertrophy is a complex anomaly of the heart associated with increased muscle mass and thickening of the cell walls in response to accumulative stress. Although this condition occurs naturally, the prolonged state will progress into heart failure or even cause death. Recent studies have revealed the eccentricity of cytochrome P450 1B1 (CYP1B1) and its associated cardiotoxic mid-chain HETEs metabolites in developing cardiac hypertrophy and heart failure. Facilitated by CYP, AA can be metabolized into several bioactive compounds such as epoxyeicotrienoic acids (EETs) and hydoyeicosatetraenoic acids (HETEs). The latter is further categorized into mid-chain, subterminal, and terminal HETEs. Subterminal HETEs have been involved in various physiological and pathophysiological processes; however, their role in cardiac hypertrophy has not been fully defined. For that reason, the objectives of the current study are; 1) to determine the possible effect of subterminal HETEs, R and S enantiomers of 16 HETE, on *CYP1B1* gene expression *in vitro* in RL-14 cells, 2) to investigate the modulatory effect of 16-HETE enantiomers *in vitro* on CYP1B1 enzyme activity medicated by human recombinant enzyme CYP1B1 and human liver microsomes, and 3) to examine the modulatory effect of 16R-HETE and 16S-HETE on different CYP450 enzyme. Our results showed that both enantiomers of 16-HETE significantly upregulated CYP1B1 at mRNA and protein levels in RL-14 cell lines. This modulation occurred through a transcriptional mechanism, as evident by transcriptional induction and luciferase assay. Furthermore, neither post-transcriptional nor post-transcriptional modification was involved in the phenomenon since there was no change in CYP1B1 mRNA and protein stability upon treatment of 16-HETE enantiomers. Surprisingly, 16-HETE enantiomers significantly increased CYP1B1 activity in RL-14 cells,

recombinant human CYP1B1, and human liver microsomes. On the contrary, 16-HETE enantiomers significantly inhibited CYP1A2 catalytic activity mediated by the recombinant human CYP1A2 and human liver microsomes. The sigmoidal binding mode of these enzyme activities represents that CYP1B1 activation occurred through allosteric regulation. In conclusion, our study provides the first evidence that 16R-HETE and 16S-HETE increase *CYP1B1* gene expression, protein through the transcriptional mechanism, and CYP1B1 at catalytic activity mediated by human recombinant CYP1B1 and liver microsome through an allosteric mechanism.

Preface

This thesis is an original work done by Mr. Rahmat Hidayat. I was responsible for designing the research, conducting experiments and data analysis as well as the manuscript composition. The homology modeling study referred to in chapter 3 was designed by Farag Mosa, with the assistance of Khaled Barakat. Dion Brocks assisted with the analysis and contributed to manuscript edits. El-Kadi AO was the supervisory author and was involved with concept formation and manuscript composition. No part of this thesis has been previously published.

This work is dedicated to

my parents, sisters and brothers.

Thank you for your conditional love and support

ACKNOWLEDGEMENTS

I wish to express my deepest gratitude and appreciation to my distinguished supervisor Dr. Ayman O. El-Kadi, for suggesting the original line of research presented in this thesis and for his trust, guidance, encouragement, and unconditional support throughout working on this research project.

I sincerely acknowledge the members of my supervisory committee, Dr. Khaled Barakat and Dion Brocks, for their endless advice and valuable suggestions.

I want to thank my former lab members, Dr. Zaid Ma'ayah and Sherif Shoieb, whose enthusiasm gave me to keep working on this research project. My special appreciation is extended to my colleagues, Mahmoud El-Ghiaty, Mohammed Alqahtani, Alammari AH, Fadumo Isse, Samar Nesr, Mohammad El-Khatib, and Sara Helal. Special thanks to Farag Mosa for his help with the computational study.

I want to thank the faculty administrative and support staff for their kind help throughout the years, with special thanks to Diseray Schamehorn, the Graduate Studies Coordinator in the faculty.

I am also grateful for the generous financial support provided by the Endowment Fund for Education (Lembaga Pengelola Dana Pendidikan (LPDP)) of Ministry of Finance, Indonesia.

This work was supported by a grant from the Canadian Institutes of Health Research (CIHR) to Ayman O. S. El-Kadi. In addition to that, I would like to thank the Faculty of Graduate Study and Research (FGSR) for supporting me with the Thesis Completion Award.

TABLE OF CONTENTS

LIST OF TABLES

LIST OF FIGURES

LIST OF ABBREVIATIONS

7-ER	7-ethoxyresorufin
AA	Arachidonic acid
AhR	Aryl hydrocarbon receptor
ANP	Atrial natriuretic peptide
BNP	B-type natriuretic peptide
COXs	Cyclooxygenases
CVD	Cardiovascular diseases
DHETs	Dihydroxyeicosatrienoic acids
DMEM	Dulbecco's Modified Eagle's Medium
DMSO	Dimethyl sulfoxide
EETs	Epoxyeicosatrienoic acids
EROD	Ethoxyresorufin O-deethylase
GAPDH	Glyceraldehyde-3-phosphate dehydrogenase GC Guanylate cyclase
GPCRs	G-protein-coupled receptors
h	Hours
HETEs	Hydroxyeicosatetraenoic acids
HF	Heart failure
LOs	Lipoxygenases
LTs	Leukotrienes
LV	Left ventricle

MROD	Methoxyresorufin O-demethylase
NADPH	Nicotinamide adenine dinucleotide phosphate
PAHs	Polycyclic aromatic hydrocarbons
PCR	Polymerase Chain Reaction
PGs	Prostaglandins
PHAHs	Polyhalogenated aromatic hydrocarbons
SDS	Sodium dodecyl sulfate
sEH	Soluble epoxide hydrolase
TCDD	2,3,7,8-tetrachlorodibenzodioxin
α- MHC	Alpha myosin heavy chain
β-MHC	Betha myosin heavy chain

Chapter 1: Introduction

1.1. Cardiac Hypertrophy and Heart Failure

Cardiac hypertrophy can be defined as a complex response of the heart towards proliferation in biochemical stress, either physiologically or pathologically, characterized by an increase in cell size and thickening of ventricular walls to normalize cardiac function (Bernardo et al., 2010a; Camici et al., 2020). Cardiac hypertrophy represents a poor prognosis of cardiac illness and is a leading risk factor for heart failure (Frey & Olson, 2003). Due to its high mortality and morbidity rates, the incidence of this cardiovascular event is increasing to 64.34 million cases worldwide and cost them 346.17 billion USD in healthcare expenditure (Lippi, 2020). Likewise, the incidence of heart failure is increasing and remains a significant economic conundrum in North America. As recorded by the Heart and Stroke Foundation of Canada, more than 669,000 Canadians live with this disease, and 50,000 new cases are being diagnosed every year. In addition to reducing the quality of life, it becomes a high economic conundrum as it causes a significant health expenditure of around $2.8 billion per year as a direct cost (Heart and Stroke Foundation, 2016).

Cardiac hypertrophy is categorized into physiological and pathological hypertrophy(Shimizu & Minamino, 2016). Physiological hypertrophy is an adaptive response that occurs naturally during a workout, in pregnancy, and in neonates (J Xiao, 2014). On the other hand, pathological hypertrophy is caused by chronic and increased pressure or volume overload in various cardiovascular conditions, including hypertension(Bernardo et al., 2010b). Should the origin fail to abate, prolonged pathological hypertrophy will be manifested in deleterious outcomes such as myocardial infection, heart failure, and even sudden death (Bernardo et al., 2010a; Stroumpoulis, 2010). Furthermore, a growing body of evidence revealed that cytochrome P450 1B1 (CYP1B1) is responsible for

the formationof cardiotoxic hydrooxyeicosatetraenoic-acid (HETE) that precipitate cardiac hypertrophy (Shoieb & El-Kadi, 2020), and several CYP enzymes, namely CYP2B2 and 2J3, exert their cardioprotection role by producing epoxyeicosatrienoic-acid EET (Aliwarga et al., 2018).

1.2. Cytochrome P450 and Arachidonic acid

Arachidonic acid (AA) is all-cis-5, 8, 11, 14-hydroperoxy-eicosatetraenoic acid with 20 carbon atoms and four double bonds in its structure, constituting the cell membrane phospholipids that can be released following the activation of cytosolic phospholipase A2 (PLA2) (Hanna & Hafez, 2018). Once released from the membrane, free arachidonic acid can be metabolized, producing several biologically active eicosanoid metabolites (Tallima & el Ridi, 2018a). Generally, two enzymes are apt to mediate AA metabolic pathways: cyclooxygenase (COX), which produces prostanoids,and lipoxygenase (LOX), producing leukotrienes, lipoxins and mid-chain HETEs (Kumar et al., 2020). However, in the last two decades, cytochrome P450 (CYP) has been widely acknowledged to have the capacity to metabolize arachidonic acid into EETs and HETEs (Anwar-mohamed et al., 2010). These three enzymes are integral membrane protein located primarily in the endoplasmic reticulum (Cojugaru et al., 2007). COX and LOX have a higher tendency to metabolize AA than CYP enzymes because the active binding sites of COX and LOX are created by a long hydrophobic channel located in the basal domain, whereas the active binding site of CYP is posited in the center of its structure, requiring some conformation changes of certain residues to bind the available ligands (Petrek et al., 2007). Nevertheless, the type of stimuli, the cofactors available, and the tissue it befalls dictate what pathway AA adopts.

CYP enzymes are a diverse group of monooxygenase enzymes that can metabolize a broad spectrum of substrates, either from the exogenous or endogenous origin, including AA (Ni & Liu, 2021). These polypeptide membrane-bound hemeproteins isoenzymes are expressed abundantly in the liver; however, they are also identified with a specific expression pattern in different organs, including the heart, kidney, lung, brain, and placenta (Cabello-Verrugio et al., 2018). In a mammal, this introductory class of enzymes is mainly located in the endoplasmic reticulum and limited expression in mitochondria (Chang & Kam, 2017).

CYP 1, 2, and 3 families mediate the metabolism of lipophilic xenobiotics such as pharmaceutical entities and carcinogens. They also contribute to the oxidative metabolism of endogenous molecules such as eicosanoids, fatty acids, and steroids. There are two phases in the xenobiotic metabolism; wherein polar functional groups are exposed or interjected into the chemical structure (phase I or activation), accompanied with the aid of the conjugation between this polar group of the xenobiotic and endogenous molecules, notably, glucuronic acid; consequently, improve its hydrophilicity (phase II or conjugation) (Westphal et al., 2015). Due to their oxidation capacity, CYP enzymes are dominantly involved in the catalysis of this phase-I reaction (Lowe Furge & Guengerich, 2006).

1.3. CYP1B1

CYP1B1 is one crucial member of the family one that is widely found in the extrahepatic tissue such as the heart and is usually correlated with a certain kind of malignant tissue (Falero-Perez et al., 2018). Along with CYP1A1 and CYP1A2, CYP1B1 plays a critical role in metabolizing a broad spectrum of xenobiotics, including activating polycyclic aromatic hydrocarbons and endobiotic including several hormones, fatty acids, melatonin,

and vitamins (Kapelyukh et al., 2019). Having this critical capacity, CYP1B1 is not only responsible for converting AA into deleterious metabolites in the cardiac tissue, but also in developing cancer. It produces carcinogenic metabolites, forms DNA adducts, and generates reactive oxygen species (ROS) (Alsubait et al., 2020).

1.3.1. CYP1B1 expressions in the cardiac tissue.

Several studies have reported the constitutive and inducible expression of CYP1B1 in the human endothelial cells and smooth muscle cells (Donway, 1998). Several studies have also reported that CYP1B1 enzyme is constitutively expressed in human adult hearts and human fetal cardiomyocytes, RL-14 cells. Albeit it is expressed constitutively, recent updates have evidenced that, when induced, CYP1B1 will demonstrate its malevolent properties by initiating various cardiovascular events(Carrera et al., 2020a), that are not limited to hypertension but can include cardiac hypertrophy and heart failure (Li et al., 2017). Therefore, CYP1B1 modulation can be a critical aspect to investigate the development of cardiac diseases.

1.3.2. CYP1B1 regulation

Numerous studies have demonstrated that CYP1B1 is regulated by aryl-hydrocarbon receptor (AhR). AhR is a basic-helix/loop/helix per-Arnt-sim (bHLH/PAS) family transcription factor (Nebert, 2017). AhR resides in the cytoplasm attached to two 90-kDa heat shock proteins (HSP90) and a 23-kDa heat shock protein (p23), along with a hepatitis B virus X-associated protein 2 (XAP2) as an inactive form (Cox & Miller III, 2004). Upon binding with a prototypic xenobiotic ligand such as 2,3,7,8-tetrachlorodibenzopdioxin (TCDD), this complex translocate into the nucleus and dissociates there, leaving AhR and

ligand alone. Then, the AhR-ligand complex associates with a close related hydrocarbon translocator (ARNT) to form a heterodimer complex (Haidar et al., 2021). This new association makes it feasible to act as a transcription factor and bind to a xenobiotic responsive element (XRE), a specific DNA recognition sequence located in the promoter region of the *CYP1B1* gene.

Each component of the AhR cytoplasmic complex holds a distinct role. Chaperon P23 protects AhR from the ubiquitylation-associated degradation during the post-translational modification and ensures AhR localization in the cytoplasm (Pappas et al., 2018). It also facilitates the association between AhR and HSP90, preventing it from developing an unexpected AhR-ARNT heterodimer complex without a ligand (Haidar et al., 2021).

It has been widely recognized that AhR can also mediate the signaling pathway for other xenobiotic metabolizing enzymes, including three other Phase-1 enzymes: CYP1A1, CYP1A2, and CYP2S1 (Nannelli et al., 2009)and Phase-2 enzymes: NADH (Nicotinamide Adenine Dinucleotide plus Hydrogen) Quinone Oxidoreductase 1 (NQO1), UDP-glucuronosyltransferase 1A6 (UGT1A6), and Glutathione S-transferase GSTA1 (Korashy et al., 2012).

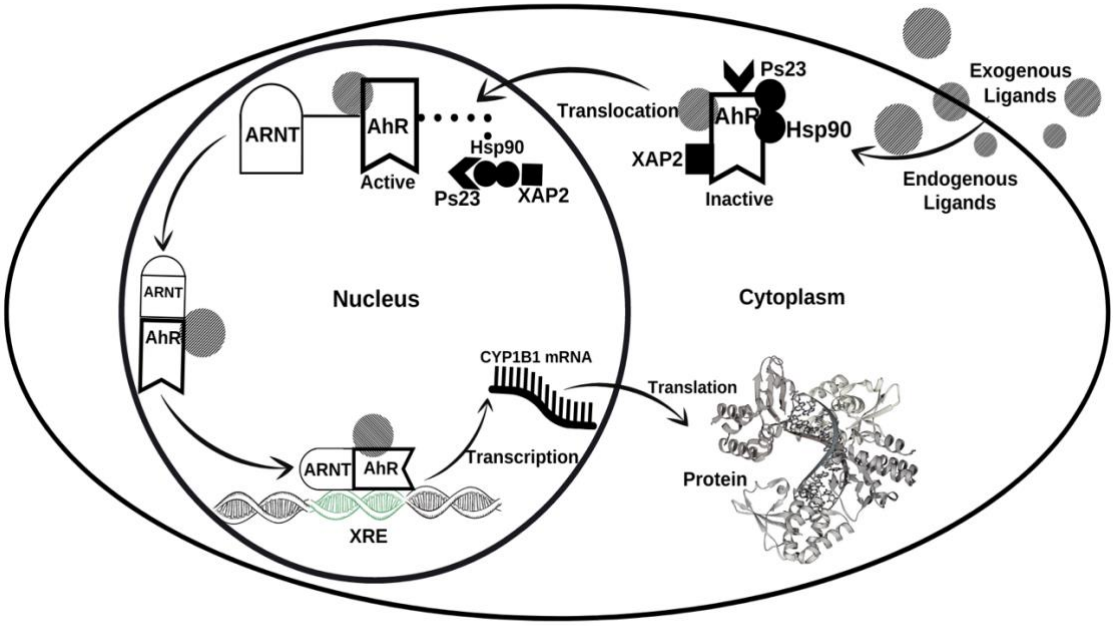

Figure 1.1. CYP1B1 is transcriptionally activated via AhR. In the classical pathway, an inactive form of the AhR is cytoplasmic and complexed with HSP90, the co-chaperone p23, and a XAP2. The AhR complex translocate to the nucleus upon binding to either endogenous or exogenous ligand. There, it dissociates and allows the AhR to form a complex with ARNT and binds to XRE in the *CYP1B1* gene, initiating the transcription process. AhR: aryl hydrocarbon receptor; ARNT: AhR nuclear translocator; and XRE: xenobiotic response element. After transcription, AhR is exported out of the nucleus to the cytosol, degraded by the ubiquitin-proteasomal pathway (Denison et al., 2011).

1.4. Mechanism involved in modulation of AhR-regulated genes

1.4.1. Transcriptional Mechanism

Generally, induction of AhR-regulated genes mainly involves de novo RNA synthesis through the transcriptional regulatory mechanism. The AhR complex will be translocated into the nucleus upon activation by endogenous or exogenous ligands. AhR will dissociate from chaperone proteins and associate with ARNT, bind to its specific binding DNA sequence, and initiate the transcription process (Figure 1.1). A study done by (Korashy & El-Kadi, 2005) revealed that the mRNA synthesis inhibitor, actinomycin-D (Act-D), inhibited heavy metals induced-cyp1a1 mRNA induction, and Jacob et al., (2011) discovered that the protein synthesis inhibitor, cycloheximide (CHX) or AhR antagonist entirely blocked diesel exhaust particles (DEP)-mediated cyp1b1 induction; suggesting that transcriptional mechanism is involved in the induction of these xenobiotic-metabolizing enzymes.

A luciferase assay can be carried out to determine whether activated AhR binds to XRE and initiate the transcription process (Satsu et al., 2015). For this purpose, the cell of interest is engineered by transfecting an XRE-driven firefly luciferase reported-gene plasmid (Smale, 2010). As the AhR is activated, it will bind to the available XRE, located toward the 5-end of the AhR regulated gene of luciferase DNA. Hence, the luciferase activity will flare up, demonstrating the transcriptional activation.

Finally, to determine the effect of a test compound on a specific gene expression, real-time Polymerase Chain Reaction (rt-PCR) can be used with specific primers for the gene of interest (Nishimura & Naito, n.d., 2013).

1.4.2. Post-transcriptional Mechanism

The steady state of protein represents the equilibrium between its synthesis and degradation rate (Rothman, 2010). Therefore, a change in degradation manner will eventually affect the steady-state concentration and the pace of its expression. Inhibiting mRNA transcription with a well-known transcription inhibitor such as Act-D that inhibits mRNA synthesis will reveal whether or not post-transcriptional mechanism is involved. The half-life of protein can be calculated, and the stability of protein of interest can be determined by plotting the decay curves against time (Elbekai and El-Kadi 2007).

1.4.3. Post-translational Modification

Post-translational modification can be defined as any functional modification toward one or more amino acids or proteins, predominantly occurring after the polypeptides once released after the original mRNA transcripts underwent translation in the ribosome (Ramazi & Zahiri, 2021). This modification can be achieved by attaching to other biochemical, functional groups such as acetate, phosphate, and various lipids and carbohydrates (Sugase et al., 2008). As a consequence, the protein functionality can be altered. There are several pathways to accomplish this modification: phosphorylation modification, proteasomal modification, and suppression by cellular heme contents, activating or inactivating the protein function (Kors, 2019).

Similar to post-transcriptional modification, inhibiting protein translation with a well-known compound such as cycloheximide that inhibits protein synthesis will reveal whether or not post-transcriptional mechanism is involved (Dai et al., 2013). The half-life of

protein can be calculated, and the stability of protein of interest can be determined by plotting the decay curves against time (Elbekai and El-Kadi 2007).

1.5. CYP-mediated Arachidonic Acid Metabolism

Various members of the CYP superfamily can metabolize omega-6 and omega-3 polyunsaturated fatty acids (n-6 and n-3 PUFAs), generating biologically active metabolites (Westphal et al., 2015). Polyunsaturated fatty acids are considered essential for cells, tissue, and organs. While linoleic acid is a parent compound of omega-6, AA (AA, 20:4, n-6) is a product formed once it is ingested into the body (Sokoła-Wysoczańska et al., 2018). AA is considered the predominant component of the membrane cells and is widely known to be metabolized by various enzymes, including CYP (Rezende et al., 2017).

Structural characterization of AA metabolites indicates that the CYP system can be subjected to three different reaction types (Rahman et al., 1997).

1. allylic oxidation to convert AA into cis, trans-conjugated "mid-chain" hydroxyeicosatetraenoic acids HETE (5-, 8-, 9-, 11-, 12- and 15-HETE) (Elkhatali et al., 2017),
2. hydroxylation near or at the terminal methyl group (ω-/(ω1)-hydroxylase reaction) generating mid-chain HETE 19-, 18-, 17- and 16-HETE; and 20-HETE (Elshenawy et al., 2013).
3. Olefin epoxidation (epoxygenase reaction) produces four benign regioisomer epoxyeicosatrienoic acids (5,6-, 8,9-, 11,12- and 14,15-EET) that are either R, S, or S, R enantiomers (Lucas et al., 2010; Spector, 2009a).

In general, the allylic oxidation reaction is attributed to CYP1B1, CYP2B, CYP2C, and CYP2J subfamilies that play their role in epoxidation.

1.5.1. CYP-derived Midchain HETEs

AA's biological significance and enzymatic biotransformation into mid-chain HETEs are not fully established. Fundamentally, mid-chain HETEs (5-, 8-, 9-, 11, 12-, and 15-HETE) are generated as the product of NADPH-AA-dependant metabolism by liver microsomes(Capdevila et al., 2000). However, many studies corroborate that various recombinants of the CYP superfamily are also responsible for producing mid-chain HETEs through an enzymatic mechanism. CYP system is capable of converting AA to the mid-chain HETEs by the hydroxylation reaction of AA while migrating the corresponding C=C double bond; or by the bis-allylic oxidation at the carbon C7, C10, and C13, followed by rearrangements of corresponding dienols (Capdevila et al., 2015; de Caterina, 2011). The bis-allyl oxidation or LOX-look reaction usually takes place under the presence of CYP1B1 (Nayyem, 2018). This enzyme is overexpressed during several cardiovascular diseases, including cardiac hypertrophy and hypertension; hence, the generation of these metabolites have been proposed as the cause of cardiovascular events (Maayah & El-Kadi, 2016). In addition to CYP1B1, mid-chain hydroxylation can be metabolized by other members of CYP systems, such as CYP1A2, which produces 5-HETE, CYP2C8 generating 11-, and 15-HETE; and CYP2C9, producing 12-, and 15-HETE (X. Liu et al., 2018).

1.5.2. CYP-derived Subterminal HETEs

Due to their oxidation capacity, CYP monooxygenases can perform a subterminal (ω-n)-hydroxylation. CYP enzymes can insert a hydroxyl functional group into terminal methyl or methylene in the AA structure. Several CYP members capable of having this reaction are CYP1A1, CYP1A2, CYP1B1, CYP2E1, CYP2F8, CYP2J, and CYP4F8. CYP1A1 oxidizes AA into 16-, 17-, 18- and 19-HETE ratios of 1.5:1:3: and 5, respectively. CYP2E1 can metabolite AA into 18-HETE and 19-HETE, constituting 32% and 49 % of the total product formed. Albeit only in minor quantities, CYP2J functions as epoxygenase and metabolize AA into 19-HETE. CYP4F8 and CYP4F12 can produce 18-HETE from AA as its primary product through ω-3 hydroxylation reaction via prostaglandin metabolism.

16-Hydroxyeicosatetraenoic acid, 16-HETE is one of the principal hydroxylated metabolites of the CYP pathway of the arachidonate cascade, although relatively little is known about its physiological actions compared with the structurally related, proinflammatory 20-HETE (Dakarapu et al., 2019).

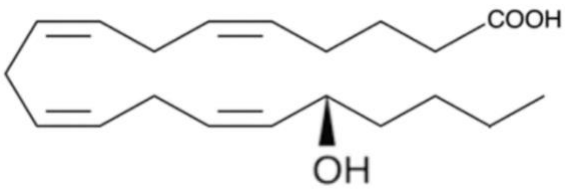

16R-(5Z,8Z,11Z,14Z,16R)-16-Hydroxyeicosatetraenoic acid

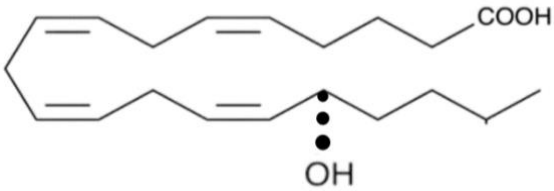

16S-(5Z,8Z,11Z,14Z,16S)-16-Hydroxyeicosatetraenoic acid

Figure 1.2. Structure 16-HETE enantiomers

1.5.3. CYP-derived Terminal HETE (20-HETE)

20-HETE is a principal metabolite after an ω-hydroxylation takes place at the omega (terminal) carbon atom of AA structure that CYP4A and 4F enzymes predominantly catalyze. Of interest, 20-HETE is the most widely recognized role in physiology and disease states (Rocic, 2018).

1.5.4. EETs

Upon PLA2 activation, the intracellular AA is metabolized via an epoxidation reaction undertaken primarily by CYP2C and CYP2J enzymes. These CYP epoxygenases introduce an oxygen atom to four susceptible double bonds of AA to form an epoxide, generating four EET regioisomers, namely 5,6; 8,9; 11,12; and 14,15 EET. Nevertheless, 11,12 and 14,15 are the primary products in many cases (Gui et al., 2020). These olefin derivatives are present in the heart, lungs, kidneys, gastrointestinal tract, and brain, with

14,15-EET mainly produced in the heart. Interestingly, the epoxide group can bind to the double bonds in the AA structure, making it feasible for each EET to generate two different configurations, R/S and S/R enantiomers.

Generally, EETs are generated in the endothelial cells; however, they can mobilize to other cells in the local environment, such as smooth muscle cells, generating their paracrine function (Spector, 2009b. Interestingly, the distribution of EET enantiomers produced by various CYP enzymes can be different significantly. Though several CYP isoforms can generate EETs in humans, the predominant CYP isoforms, CYP2C8, CYP2C10 and CYP2J2, are expressed in the endothelium. CYP2C8-derived EETs constitute 82 percent R/S, while CYP2C10 only generates 69 percent S/R. Surprisingly, in endothelial cells, CYP2J enzyme can produce a different quantity of two regioisomers; for example, although CYP2J2 produces both 11,12-EET and 14,15 EET, the former is a racemic mixture, while the latter constitutes 75 percent in R/S enantiomers (Spector & Norris, 2007).

Numerous studies have investigated the beneficial effect of EETs. These CYP-epoxygenases derivatives have been proclaimed to have vasodilation, anti-inflammation, and anti-platelet aggregation properties to combat cardiovascular diseases (Franchina et al., 2018). Increasing evidence suggests that EETs play an essential role in cardioprotective mechanisms; they are potent vasodilators proposed to function as an endothelium-derived hyperpolarizing factor (EDHF) in some tissues. Most importantly, EETs could contribute to neovascularization by promoting angiogenesis (Waldman et al., 2016).

EETs has to undergo another metabolic fate. Soluble epoxide hydrolase (sEH) metabilize EETs into corresponding vicinal diols (Samokhvalov et al., 2019), the dihydroxyeicosatrienoic acids (DHETs), through hydration reaction ((W. jun Liu et al.,

2015). These derivatives are considered less biologically than their corresponding parent compounds (Yang et al., 2013).

1.5.5. The role of CYP-derived AA in cardiac hypertrophy and heart failure

The terminal HETE, 20-HETE, has been widely acknowledged to have detrimental effects on the cardiovascular system, including endothelial cell dysfunction and inflammation. For instance, Althurwi et al. (2015) reported a significant increase in CYP ω-hydroxylase and its associated metabolite, 20-HETE, in the isoproterenol-induced cardiac hypertrophy in vivo.

Furthermore, myriads of studies have reported the increased formation of cardiotoxic mid-chain HETES in monocytes, vascular smooth muscle cells, and endothelial cells, prompting the development of various cardiovascular dysfunction such as atherosclerosis, hypertension, cardiac hypertrophy, and heart failure. Maayah and El-Kadi (2017) were the first to report that mid-chain HETE induced cardiac hypertrophy markers such as Atrial Natriuretic Peptide (ANP), Brain Natriuretic Peptide (BNP), α-, and β-Myosin Heavy Chain (MHC) in RL-14 cells, thus causing cellular hypertrophy as evidenced by a significant increase in cell size. In an effort to understand the phenomenon, they found that cellular enlargement was associated with the capacity of mid-chain HETEs to induce NF-κB activity and ERK1/2 phosphorylation. In addition to that, in a mono-center retrospective nested case-control study, Zu et al. reported that plasma levels of 8-HETE, 11-HETE, 12-HETE, and 15-HETE were significantly increased in people with the acute coronary syndrome in the presence of major adverse cardiovascular events such as heart failure and myocardial infarction. In addition, El-Sherbeni and El-Kadi (2014) reported increased formation of 5-HETE, 12-HETE, and 15-HETE in pressure-overload induced cardiac hypertrophy rat

model. 12-HETE is one of the major mid-chain metabolites produced in the vasculature. It is reported to pose a concentration-dependent vasoconstriction, with threshold concentration of 10^{-9} M, when investigated in the dog's isolated perfused arcuate renal arteries using video microscopy (Ma, 1991). It could reduce the vascular diameter from 306 to 63 μm, representing 37% of maximum vasoconstrictor response to epinephrine. Similarly, 15-HETE had also been reported to increase the sensitivity of isoproterenol-mediated by the β-adrenergic response in rat neonatal cardiomyocytes (Maayah et al., 2017).

Interestingly, unlike mid-chain HETEs, the role of subterminal HETEs on cardiac hypertrophy has not been fully established—however, several significant discoveries have led us to draw a bigger picture. For example, Shoieb and El-Kadi (2019), reported that 19S-HETE could significantly inhibit the CYP1B1 activity when mediated by recombinant human CYP1B1 enzyme and liver microsomes, and it prevented the angiotensin II-induced cellular hypertrophy in RL-14 and H9c2 cells (Shoieb et al. 2018). As for the other subterminal HETEs, there were no reports underlying the role of 18-HETE, 17-HETE, and 16-HETE on cardiac hypertrophy and heart failure.

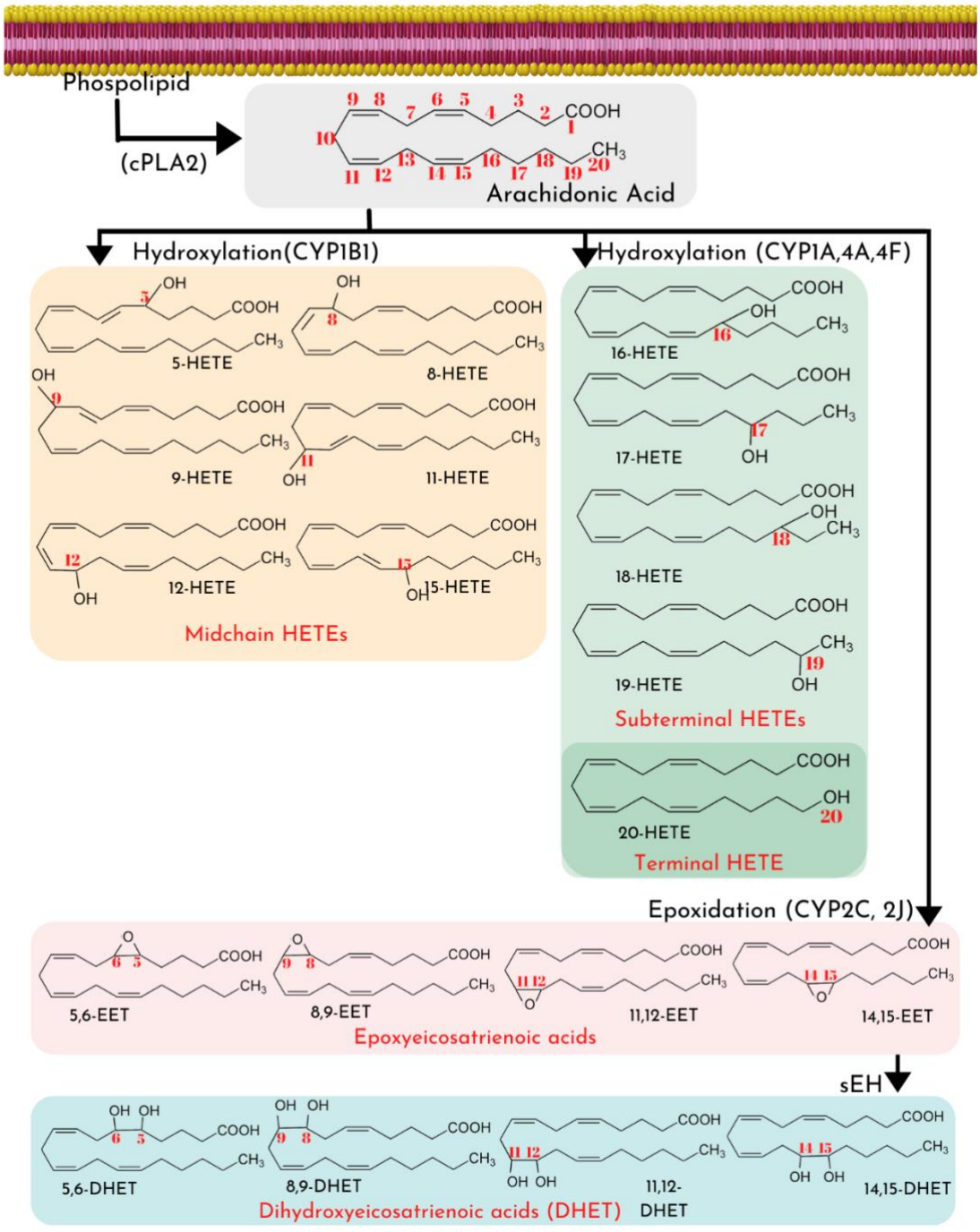

Figure 1.3. CYP pathway of arachidonic acid metabolism. Arachidonic acid is released following activation of phospholipase A2 and subsequent metabolism by CYP pathways. These enzymes insert oxygen at different positions in AA to generate a major family of biologically active mediators called eicosanoids.

1.6. Enzyme Allostery

1.6.1. Allostery in CYP

Allostery of CYP enzymes has also been recognized since the last decade. Despite the controversy of its significance and location, several shreds of evidence have corroborated that CYP elucidates atypical enzyme kinetics originating from its peripheral allosteric binding site (Polic et al., 2018). One important instance of this peculiar phenomenon is shown by CYP3A4, where it experiences allosteric activation upon progesterone treatment (Polic & Auclair, 2017).

1.6.2. Allosteric activation and inhibition.

Classically, enzyme activity, particularly enzyme inhibition, results from competitive interaction between a substrate and a ligand to sit on the enzyme's active binding site, known as an orthosteric site. However, the function of an enzyme could also be altered when the interaction occurs in another available yet suitable binding site, known as an effector or allosteric site (di Cera, 2009).

The enzyme binding site favors two configurations: high affinity or relaxed (R) state and low affinity or taut (T) state. A study done by Iwata et al. (2009), demonstrated that a conformational change at the effector site rearranges these configurations, initiating the allosteric activation. They witness a concerted rotation between the T-state into the R-state of the tetramer subunits of bacterial L-lactate dehydrogenase, following the allosteric activation, thus modifying the substrate affinity. Interestingly, under profound scrutiny, it is revealed that a particular amino acid constituted in the effector site is responsible for the allosteric stimulation. For instance, through molecular dynamic simulations, (Denisov et al.,

2019) discovered that a phenylalanine residue (Phe213) was accountable for the allosteric activation of CYP3A4 by progesterone. Interestingly, other suitable amino acids may trigger this atypical kinetic, increasing enzyme activity (Robinson, 2015).

Nonetheless, when the interaction between ligand and amino acid domain shifts the R-state into the T-state, the activity of the enzyme declines, representing an allosteric inhibition (Johnson et al., 1997). An experiment by (Kotaka et al., 2006) best explains this scenario; the binding between amino acid lysine with the regulatory ACT domain of Aspartokinase III (AKIII) from Escherichia coli disrupts the R state and bolsters the T-state of the enzyme, causing a rotational rearrangement, and thus reducing AKIII activity.

In addition to that, the capacity of fatty acids to modulate allostery has been reported previously (Dong et al., 2016). They reported that fatty acid mediates cyclooxygenase-2 inhibition by binding to the allosteric subunits (E-allo) of this enzyme, similar to other COX-2 inhibitors: naproxen and flurbiprofen (Dong et al., 2016).

Allosteric regulation occurs mainly when the protein or enzyme poses more than one subunit. A typical example of this phenomenon is the allostery of human hemoglobin (HbA), which is an oxygen transport protein composed of two α and two β subunits (Resbech, 2013). Under allosteric regulation, it is widely accepted that O2 acts as a "site-specific" homotropic allosteric effector trigger the quaternary change from the low O2 affinity T state to the high-affinity R one (Takayanagi, 2014).

1.7. Rationale, Hypothesis, and Objectives

1.7.1. Rationale

Cardiac hypertrophy is a convoluted manifestation of a heart, associated with increased cardiac mass due to enlargement and thickening heart walls. It is a natural response towards an increased stimulus such as pressure overload yet becomes deleterious if the trigger remains untreated. Prolonged pathological hypertrophy can progress into heart failure or other heart conditions. The prevalence of this condition grows every year and becomes a global pandemic representing a leading cause of morbidity and mortality worldwide.

A growing body of evidence reveals that cardiac hypertrophy is strongly correlated with CYP1B1, constitutively expressed and inducible in the cardiac tissue. Several studies have reported that the induction of this enzyme will facilitate the production of cardiotoxic mid-chain HETE (5-, 8-, 12-, and 15-HETE); thus, promoting the development of cardiovascular events. For instance, these malevolent metabolites have been linked to the development of cardiac hypertrophy.

Of interest, 20-HETE has become the most CYP-derived AA metabolite that has been well established to be involved in cardiac hypertrophy and heart failure. On the other hand, subterminal HETEs such as 19-, 18-, 17-, and 16-HETE received less attention; despite the fact that their peculiar feature for having R and S enantiomers. Among these subterminal HETEs, 16-HETE received the least attention, whereas the position of the oxidative functional group is the closest to the mid-chain HETE. This raises the question of whether 16-HETE will alter CYP1B1expression and, in turn, corroborate mid-chain formation.

1.7.2. Hypothesis

1) 16R-HETE and 16S-HETE modulate CYP1B1 gene expression and enzyme activity in a concentration-dependent manner in-vitro in RL-14 cells, and

2) 16R-HETE and 16S-HETE alters the activity of several CYP differentially, presumably through an allosteric mechanism.

1.7.3. Objectives

The specific objectives of this study are to:

1) determine the possible effect of 16R-HETE and 16S-HETE on *CYP1B1* gene expression in vitro in RL-14 cells,

2) investigate the modulatory effect of 16-HETE enantiomers *in vitro* on CYP1B1 enzyme activity medicated by human recombinant enzyme CYP1B1 and human liver microsomes, and

3) examine the modulatory effect of 16-HETE enantiomers on another CYP enzyme.

Chapter 2: Materials and Methods

2.1 Chemicals and Materials

16R-HETE and 16S-HETEs were purchased from Cayman Chemical (Ann Arbor, MI, USA). Dulbecco's Modified Eagle's Medium/F-12 (DMEM/F- 12) and DMEM were purchased from Gibco, Life Technologies (Grand Island, NY, USA). Fetal bovine serum (FBS) was obtained from Sigma-Aldrich Co. (St. Louis, MO, USA). TRIzol reagent was obtained from Invitrogen Co. (Carlsbad, CA, USA, and High Capacity cDNA RT (Reverse-Transcription) Kit. SYBR® Green PCR Master Mix was obtained from Applied Biosystems (Foster City, CA, USA). Primers for real-time PCR analysis were formulated and obtained from Integrated DNA Technologies (Coralville, IA, USA). Immun-Blot® PVDF membrane was obtained from Bio-Rad Laboratories (Hercules, CA, USA). Beta-Actin and recombinant monoclonal anti-CYP1B1 antibodies were purchased from Abcam (Toronto, ON). Detection reagents for a Chemiluminescence Western blotting were obtained from GE Healthcare Life Sciences (Pittsburgh, PA, USA). 16(R)-, 16S-HETEs, were purchased from Cayman Chemical (Ann Arbor, MI, USA). 7-ethoxyresorufin (7-ER), 7-methoxyresorufin (7-MR), and nicotinamide adenine dinucleotide phosphate (NADPH) tetrasodium salt were purchased from Sigma Chemical Co. (St. Louis, MO). Human recombinant CYP1A2 and CYP1B1 microsomes supplemented with NADPH–cytochrome P450-oxidoreductase (Corning-SupersomesTM) were obtained from Fisher Scientific (Hampton, NH). InVitroCYP TM human liver microsomes were purchased from BioIVT (Hicksville, NY, USA).

2.2. Cell culture

Human fetal ventricular cardiomyocyte (RL-14) cells were obtained from American Type Culture Collection (ATCC) (Manassas, VA, USA). These cells were maintained in DMEM/F-12 plus phenol red supplemented with 12.5% FBS, 20μM l-glutamine, and 1% penicillin-streptomycin. The cells were grown in a 75 cm2 culture flask at 37 °C in a 5% CO2 humidified environment. Each 75 cm2 flask had an average of 7.5 x 106 cells. For seeding, each well in the 6-well plate contained an average of 9.5 x 105 cells, each well in the 12-well plate contained an average of 3.8 x 105 cells, and each well in the 24-well plate contained an average of 1.9 x 105 cells.

2.3. Chemical treatment

To evaluate the modulatory effects of 16-HETE enantiomers, cells were treated with vehicle constituting serum-free DMEM/F12 and supplemented with 0.05% DMSO or 20 μM of either 16R-HETE or 16S-HETE in SFM (serum-free medium) over the course of the experiments (see figure legends). 16R-HETE or 16S-HETE was supplied as a stock solution in DMSO and kept in DMSO at −20 °C. mRNA assay was performed in 12-well cell culture plates whereas protein assay was carried out in 6-well cell culture plates. To investigate the effect of 16R-HETE or 16S-HETE on cardiac hypertrophic and inflammatory markers, cells were treated in the absence or presence of 20 μM 16R-HETE or 16S-HETE for 24 h as described in the figure legends. 16R-HETE or 16S-HETE stock solutions were freshly prepared in serum-free medium (SFM) before each experiment. In all experiments the DMSO concentration did not exceed 0.05% (v/v).

2.4. Measurement of cell viability

The viability of RL-14 cells was measured using an MTT assay. This assay depends on the ability of viable cells to reduce tetrazolium dye MTT 3-(4,5- dimethylthiazol-2-yl)-2,5-diphenyltetrazolium bromide to its insoluble colored formazan crystals. Initially, cells were seeded in 96-well plates, incubated with 16-HETE enantiomers for 24 h at 37 °C in a 5% CO2 humidified incubator to reach sufficient confluency. After that, cells were incubated with 1.2 mM MTT (20 µl/well) dissolved in phosphate-buffered saline (PBS; pH 7.4) for three h at 37 °C, and then the formazan crystals were dissolved for 10 min at room temperature with 150 µl/well isopropyl alcohol. The optical density was then measured by light absorbance using a wavelength of 550 nm using the Bio-Tek Synergy H1Hybrid Multi-Mode Microplate Readers (Bio-Tek Instruments, Winooski, VT, USA). The proportion of healthy cells was expressed as a percentage of the control mean absorbance value.

2.5. Measurement of cell surface area

Relative changes in cell surface area in response to treatments, as an indicator for hypertrophy, were measured using phase-contrast imaging, which was taken with a Zeiss Axio Observer Z1 inverted microscope using the 20X objective lens as described previously (Zordoky et al., 2010b; Tse et al., 2013). Briefly, RL-14 cells were treated with test compounds for 24 h; then, phase-contrast images were taken with Zeiss Axio Observer Z1 inverted microscope using the 20X objective lens. The surface area was then quantified by imaging the complete boundary of individual cells with Zeiss AxioVision software (Carl Zeiss Imaging Solutions). Five different images were taken, and fifty cells were counted for each treatment group.

2.6. Assessment of CYP1B1 enzymatic activity

Enzymatic activity of CYP1B1 was determined by a 7-ethoxyresorufin O-demethylase (EROD) assay, which was performed on intact living RL-14. Briefly, cells were seeded in 24-well plates. Then, ethoxyresorufin (2 μM) and either 16R-HETE or 16S-HETE were added in assay buffer (0.05 M Tris, 0.1 M NaCl) with pH=7.8. The experiment was initiated with a fluorescence measurement (t = 0) at excitation/emission wavelengths (535/585 nm), respectively. Fluorescence of the samples was recorded every 5 min interval for 40 min using the Bio-Tek Synergy H1 Hybrid Multi-Mode Microplate Readers (BioTek Instrument, Winooski, VT, USA). The quantity of resorufin formed of each sample was assessed by comparing it to a standard curve of known concentrations. Using a fluorescence-based protein assay, the CYP1B1 enzymatic activity was assessed by normalizing it to protein content in the cells (Lorenzen and Kennedy, 1993).

2.7. RNA extraction and cDNA synthesis

Total RNA from cells was isolated using a TRIzol reagent (Invitrogen®) as directed by the manufacturer's instructions. The quantity of isolated RNA was determined by measuring the absorbance at 260 nm, and the purity was confined by measuring the 260/280 ratio (>1.8). After that, first-strand cDNA synthesis was conducted using the High-Capacity cDNA reverse transcription kit (Applied Biosystems) as the manufacturer instructed. Shortly, 1.5 μg of total RNA from each sample was added to an amalgam containing 2.0 μl 10× reverse transcriptase (RT) random primers, 0.8 μl 25× dNTP mix (100 mM), 2.0 μl 10× RT buffer, 1.0 μl MultiScribeTM reverse transcriptase enzyme, and 4.2 μl nuclease-free

water. The final reaction mixture was maintained at 25 °C for 10 min, heated to 37 °C for 120 min and followed by 85 °C for 5 min, and cooled down to 4 °C.

2.8. Real-time polymerase chain reaction (real-time PCR) for quantification of mRNA expression

Real-time PCR was utilized to determine the specific quantity of mRNA expressions of distinct targets by subjecting the cDNA to PCR amplification using a of 384-well optical reaction plates in the Applied BiosystemsTM Quant Studio 5 Real-Time PCR System. The reaction mixture (20 µl) contained 0.04 µl of 10 µM forward primer and 0.04 µl of 10 µM reverse, 10 µl of SYBR Green Universal Master mix, 8.92 µl of RNAse/DNAse-free water, and 1 µl of cDNA sample. Human primer sequences for CYP1B1, ANP, α-MHC, β-MHC, and β-actin, as well as rat primer sequences for CYP1B1, ANP, BNP, α-MHC, β-MHC, and β-actin, are listed in (Table 2.1). PCR Primers were designed and obtained from Integrated DNA technologies IDT (Coralville, IA, USA). The real-time PCR data were analyzed using the relative fold gene expression (i.e., ΔΔ CT) method. In brief, the change in the level of target genes between treated and untreated cells and corrected for the level of a housekeeping (reference) gene (β-actin) were set using the following formula: mRNA fold change = $2^{-\Delta(\Delta Ct)}$, where ΔCt = Ct (target) − Ct (housekeeping gene) and Δ(ΔCt) = ΔCt (treated) – ΔCt (untreated). The thermal cycle frameworks were as follows: the reaction was initiated at 95°C for 10 min and followed with 40 cycles of denaturation (95°C, 15s) and combined annealing/extension (60°C, 60s).

Table 2.1. Primer sequences used for RT- PCR reactions.

Genes	**Reverse primer**	**Forward primer**
CYP1B1	TTCGGCCACTACTCGGAGC	CAGAAGCTGCTGGAGCTGATAAG
ANP	AGCCCCCGCTTCTTCATTC	CAACGCAGACCTGATGGATTT
BNP	TGTAGGGCCTTGGTCCTTTG	ACAGAGTGCTTCGTGCCTGAT
α-MHC	GCCCTTTGACATTCGCACTG	GCCCTTTGACATTCGCACTG
β-MHC	TCACCAACAACCCCTACGATT	TCACCAACAACCCCTACGATT
β-actin	CTGGCACCCAGCACAATG	ACCAGTTCCTGAATGGCTGC

2.9. Protein extraction

RL-14 cells were grown in 6-well plates and incubated with the test compounds for 24 h. Afterward, lysis buffer constituted by 50 mM HEPES, 1.5 mM magnesium chloride, 0.5 M sodium chloride, 1 mM EDTA, 10% (v/v) glycerol, 5 µl/mL protease inhibitor cocktail, and 1% Triton X-100 were used to collect the cell lysates. Afterward, the cell lysates were subjected to incubating on ice for one h to prepare the cell homogenates with a sporadic vortex every 10 min, followed by centrifugation at 12,000 × g for 10 min at 4°C. Then, the supernatant of total cellular lysate was collected and maintained at −80°C. After that, the Lowry method was used to determine the protein concentration using bovine serum albumin as a standard (Lowry et al., 1951).

2.10. Western blot analysis

Western blot analysis was performed according to a previously detailed assay. Briefly, proteins from each group were separated by 10% sodium dodecyl sulfate-polyacrylamide gel electrophoresis (SDS–PAGE), samples underwent electrophoresis at 120 V for two h, and separated proteins were transferred onto Immun- Blot® PVDF membranes. Afterward, protein membranes were blocked to prevent non-specific binding overnight at 4 °C using in blocking solution containing 3 mM potassium chloride, 0.15 M sodium chloride, 25 mM Tris-base, 2% bovine serum albumin, 5% skim milk, and 0.5% Tween 20. Following blocking, the blots were washed 3 times for 15 min with buffer TBS (Tris-buffered saline)–Tween-20. The blots were subsequently incubated with primary antibodies in TBS solution (0.05% (v/v) Tween-20, 0.02% sodium azide) for 2 h or as indicated at 4 °C. Incubation with secondary antibodies (peroxidase-conjugated IgG) in blocking solution was performed for

30-45 min at room temperature. According to the manufacturer's guide, the bands were visualized using the enhanced chemiluminescence method (GE Healthcare Life Sciences). To quantify the intensity of protein bands concerning the signals acquired from GAPDH loading control, the membrane was placed and analyzed using ImageJ software (National Institutes of Health, Bethesda, MD, USA; http://rsb.info.nih.gov/ij). The results' data are represented as relative protein intensity (%) + SEM compared to the control group.

2.11. Luciferase Assay

Recombinant HG2L7.5c1 human hepatoma cells stably transfected with an Ah receptor-responsive firefly luciferase reporter gene plasmid, pGudluc7.5 (which contains 20 dioxin responsive elements) were used.

(Brennan et al., 2015). The transfected HG2L7.5c1 human hepatoma cell was generously provided by Dr. M. S. Denison (University of California, Davies). The luciferase assay was performed according to the manufacturer's instructions (Promega) and reported as a relative light unit (RLU). In brief, transfected HepG2 were seeded in 48 well-plate and incubated for 24 h. Moreover, cells were incubated with 16-HETE enantiomers or TCDD (1 nM) for 24 h. To each plate well, add 75µl of Dual-Glo® reagent equal to medium in the well and mix. In this assay, bioluminescence is produced by converting the chemical energy of luciferin oxidation through an electron transition, forming the product molecule oxyluciferin. Wait at least 10 min to allow for cell lysis to occur, then measure the firefly luminescence using a BioTek Synergy H1 Hybrid Reader (BioTek Instruments, Inc.).

2.12. CYP1B1 mRNA Stability

The half-life of CYP1B1 mRNA was analyzed by the Act-D-chase assay. mRNA half-life ($t_{1/2}$) is defined as the interval of time required for one-half (50%) of the mRNA of a total initial sample to decay. The half-life of a first-order reaction is a constant that is related to the rate constant for the reaction: $t_{1/2} = 0.693/k$ (where k= slope). To determine the effect of 16-HETE enantiomers on the CYP1B1 mRNA t1/2 at the constitutive level, cells were treated with Act-D (5 μg/mL) for 30 minutes to inhibit further RNA synthesis immediately before treatment with EITHER 16R-HETE or 16S-HETE, or TCDD (1 nM). After that, total RNA was extracted at 0, 1, 3, 6, 12, and 24 h post-treatment.

To determine the effect of 16-HETE enantiomers at the inducible level, cells were pre-treated with TCDD (1 nM) for 6 h. After that, cells were washed three times and incubated with Act-D (5 μg/mL) for 30 min before treatment with the test compound. Total RNA was extracted at 0, 1, 3, 6, and 12 h after incubation with the test compound. Real-time PCR reactions were performed as described in the materials and methods section. The mRNA t1/2 values were determined from semilog plots of mRNA amounts and expressed as a percentage of treatment at t = 0 versus time.

2.13. CYP1B1 Protein Stability

The CHX-chase assay analyzed the t1/2 of CYP1B1 protein. Protein half-life ($t_{1/2}$) is defined as the interval of time required for one-half (50%) of the protein of a total initial sample to decay. The half-life of a first-order reaction is a constant that is related to the rate constant for the reaction: $t_{1/2} = 0.693/k$ (where k= slope). Cells were pretreated with TCDD

(1 nM) for 24 h. Afterward, cells were washed three times with serum-free media and incubated with CHX (10 μg/mL) to inhibit further protein synthesis immediately before treatment with 16-HETE enantiomers). Cell homogenates were extracted after incubation with the 16-HETE enantiomers at several time points. CYP1B1 protein was measured by Western blotting as described previously, and the protein t1/2 values were determined from semilog plots of integrated densities versus time.

2.14. Determination of CYP1B1 modulatory-kinetics by 16-HETE enantiomers

The O-dealkylation rate of 7-ER (EROD) by recombinant human CYP1B1 was measured in the absence or presence of 16R-HETE or 16S-HETE. Briefly, the fluorescent assay was carried out in a 96-well solid black polystyrene microplate. The reaction mixture contains 100 mM potassium phosphate (pH 7.4) buffer plus 5 mM magnesium chloride hexahydrate, and 1 pmol of human recombinant CYP1B1 (EROD) were incubated with an increasing concentration of 7-ER (10- 100 nM). After that, 0, 5, 10, 20, or 40 nM of either 16R-HETE or 16S-HETE was added to the reaction amalgamation. To run the experiment, 100 μL of the reaction mixture was utilized. The reaction was commenced as 100 μL of 2 mM NADPH was added to the reaction mixture; then, the fluorescent signal related to the formation of resorufin was measured using a BioTek Synergy H1 Hybrid Reader (BioTek Instruments, Inc.) every min for 30 min at 37°C (550 and 585 nm were selected as excitation and emission wavelengths, respectively). The amount of product formation (resorufin) was measured by constructing a standard curve of concentrations (0-200 nM) of resorufin dissolved in the same working incubation buffer. The resorufin formation rate in each well was determined using linear regression over the first 9 min period. The rate of resorufin

formation at different 7-ER concentrations was fitted to the Michaelis-Menten equation. After that, the results of 16-HETE enantiomers on CYP1B1 induction rates were fitted to the most suitable model: sigmoidal-Michaelis Menten. The fitting was performed using GraphPad Prism (version 5.01; GraphPad Software, Inc., La Jolla, CA) and Microsoft Excel solver.

2.15. Determination of CYP1A2 inhibitory-kinetics by 16-HETE enantiomers

The O-dealkylation rate of MR (MROD) by recombinant human CYP1A2 was measured in the absence or presence of 16R-HETE or 16S-HETE. Briefly, the fluorescent assay was carried out in a 96-well solid black polystyrene microplate. The reaction mixture contains 100 mM potassium phosphate (pH 7.4) buffer plus 5 mM magnesium chloride hexahydrate, and 1 pmol of human recombinant CYP1A2 were incubated with an increasing concentration of MR (10- 100 nM). After that, 0, 5, 10, 20, or 40 nM of either 16R-HETE or 16S-HETE was added to the reaction amalgamation. To run the experiment, 100 µL of the reaction mixture was utilized. The reaction was commenced as 100 µL of 2 mM NADPH was added to the reaction mixture; then, the fluorescent signal related to the formation of resorufin was measured using a BioTek Synergy H1 Hybrid Reader (BioTek Instruments, Inc.) every min for 30 min at 37°C (550 and 585 nm were selected as excitation and emission wavelengths, respectively). The amount of product formation (resorufin) was measured by constructing a standard curve of concentrations (0-200 nM) of resorufin dissolved in the same working incubation buffer. The resorufin formation rate in each well was determined using linear regression over the first 9 min period. The rate of resorufin formation at different MR concentrations was fitted to the Michaelis-Menten equation. After that, the results of

16-HETE enantiomers on CYP1B1 inhibition rates were fitted to the most suitable model: sigmoidal-Michaelis Menten. The fitting was performed using GraphPad Prism (version 5.01; GraphPad Software, Inc., La Jolla, CA) and Microsoft Excel Solver.

2.16. Assessment of CYP1B1 and CYP1A2 enzymatic activities in human microsomes

Enzymatic activity of CYP1B1 and CYP1A2 was determined by EROD and MROD assays, respectively, using human liver microsomes polled from 25 different individuals in the absence and presence of 16R-HETE or 16S-HETE. Briefly, the 96-fluorescent assay was carried out using 96-well solid black polystyrene microplates. The reaction mixture contains 100 mM potassium phosphate (pH 7.4) buffer supplemented with 5 mM magnesium chloride hexahydrate, 0.2mg/ml human liver microsomes, and 2 μM of 7-ER for EROD assay or 5 μM of 7-MR for MROD assay. In addition, 0, 20, 40, 80, or 100 nM of either 16R-HETE or 16S-HETE was added to the mixture. In this experiment, the volume of the reaction mixture was 100 μL. The reaction was started by adding 100 μL of 2 mM NADPH to the amalgam. The fluorescent signal related to the formation of resorufin was measured every min for 20 min at 37°C (excitation and emission wavelengths were assigned as 550 and 585 nm, respectively) using a BioTek Synergy H1 Hybrid Reader (BioTek Instruments, Inc) using a BioTek Synergy H1 Hybrid Reader (BioTek Instruments, Inc.). The calculation of IC50 and the fitting of data were performed using GraphPad Prism (version 5.01; GraphPad Software, Inc., La Jolla, CA) using the concentration-response inhibition module. In clinical settings, CYP1A2 plays an important role in metabolism of drugs like clozapine, olanzapine, fluvoxamine, haloperidol, theophylline; whereas, CYP1B1 is responsible for the metabolism of several anticancer drugs such as docetaxel, paclitaxel, mitoxantrone and flutamide.

2.17. Prediction of CYP1B1 binding pockets

The available pockets were predicted using Molecular Operating Environment (MOE) software. First of all, the protein preparation was carried out by loading the reported CYP1B1 crystal structure, 6IQ5, that was adopted from Protein Data Bank (PDB) into MOE to add the missing residue and loop, and to sign the right protonation at pH 7. Thereafter, the site finder will assign the possible cavity/binding pockets based on the suitable algorithm. The molecular surface colored by atom colors.

2.18. Data and statistical analysis

All results are presented as the mean ± SEM. Multiple group comparisons were performed using one-way analysis of variance (ANOVA) followed by the Student–Newman–Keuls as a post hoc test. Differences between means were considered significant at $p < 0.05$. All analyses were performed using GraphPad Prism® for Windows (Systat Software, San Jose, CA, USA). Km, Vmax, and IC_{50} values were determined using the Enzyme Kinetics module from GraphPad Prism, version 8.01, and Microsoft Excel Solver. Microsoft Excel Solver defined the corresponding Hill coefficient (n) that represents the degree of cooperativity (allostery). Nonlinear regression analysis and fitting to simple or sigmoid Michaelis-Menten equations were applied, the most probable mode of binding was selected based on the measures of goodness of fit, including r2 between the observed and fitted values and the sum of squares of the differences. The fitting was applied to the following equations:

Simple Michaelis-Menten model:

$$v_{resorufin} = \frac{V_{max} \text{ x } C_{ethoxyresorufin}}{K_m + C_{ethoxyresorufin}}$$

Sigmoidal Michaelis-Menten model:

$$v_{resorufin} = \frac{V_{max\ n} \text{ x } C_{ethoxyresorufin}}{K_m{}^n + C_{ethoxyresorufin}}$$

Vmax is the maximum velocity rate of resorufin formation; km is the affinity constant, C is the substrate concentration, n is the Hill coefficient. The CL_{int} was calculated by dividing the V_{max} by the K_m.

$$CL\text{int} = \frac{Vmax}{Km}$$

To determine mRNA and protein half-life, all decay curves were analyzed individually. The half-life was estimated from the slope of a straight line fitted by linear regression analysis ($r^2 \geq 0.85$) to a semilog plot of protein amount to obtain following function:

$$y = A_0 e^{-kt}.$$

where A_0 is the starting value, *e* is Euler's constant and k is a negative constant that determines the rate of decay. After that, half-life was determined using following equation:

$$Half - life\ (t\frac{1}{2}) = \frac{\ln(2)}{k} = \frac{0.693}{k}$$

Chapter 3: Results

3.1. The effect of 16 HETE enantiomers on hypertrophic markers and human *CYP1B1* gene expression, protein expression, and activity.

3.1.1. Effect of co-exposure to 16R-HETE and 16S-HETE on cell viability

The cytotoxicity was assessed using the MTT assay as described in the materials and methods. Our results showed that neither 16R-HETE nor 16S-HETE, at the tested concentrations, significantly affected cell viability of the RL-14 cells compared to control (depicted by the viability above 90%). Based on this finding, 20 μM was selected to carry out all subsequent experiments as it was demonstrated to be safe by the MTT assay (Figure 3.1.1).

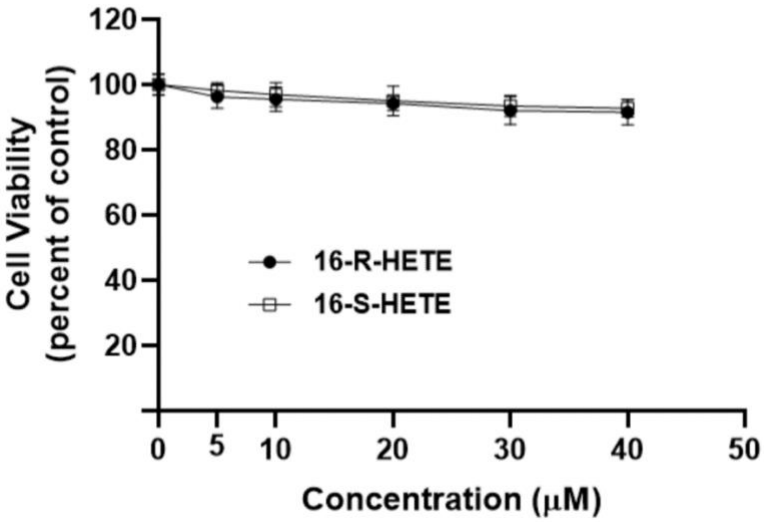

Figure 3.1. 1. Effect of 16R-HETE and 16S-HETE on cell viability. Human RL-14 cells were treated with increasing concentrations of 16-HETE enantiomers for 24 h. Data are expressed as the percentage of untreated control (set as 100 %) ± SE (n=6).

3.1.2. Effect of 16-HETE enantiomers on hypertrophic markers.

To evaluate the capacity of 16R-HETE and its enantiomer to induce cellular hypertrophy, RL-14 cells were co-exposed to 20 μM of 16R-HETE and 16S-HETE for 24 h; and the expressions of cardiac hypertrophic markers: α-MHC, β-MHC, ANP, and BNP were measured accordingly using real-time PCR.

Our results showed that the treatment significantly increased all hypertrophic markers. As shown in figure 3.1.2 A, α-MHC and β-MHC were modulated by 16R-HETE up to 48.3 and 23.1 percent, respectively, compared to control: giving the β/α MHC ratio of 2.009. Albeit having a lower capacity than its enantiomer, 16S-HETE could also significantly increase α-MHC and β-MHC mRNA expression up to 2.7 and 6.2 percent, respectively.

Similarly, a significant increase in ANP and BNP mRNA expressions was observed in the human fetal cardiomyocytes following the incubation of 16-HETE enantiomers for 24 h. The optimum inductions of ANP and BNP mRNA by 16R-HETE were recorded as 5.12 and 7.82 folds, respectively. However, 16S-HETE, though still significant, could induce these hypertrophic markers up to 3.62 and 3.05, respectively (Figure 3.1.2.B).

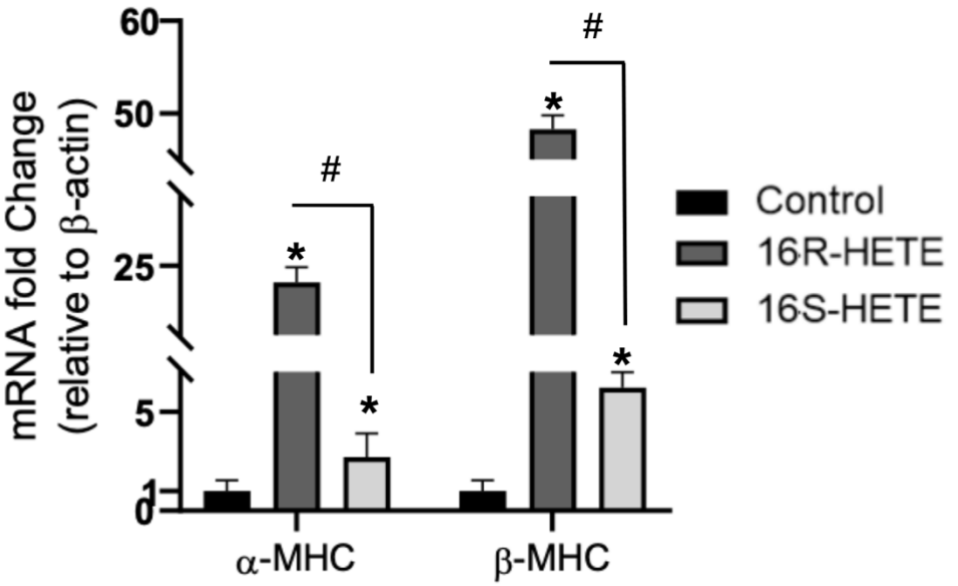

(A)

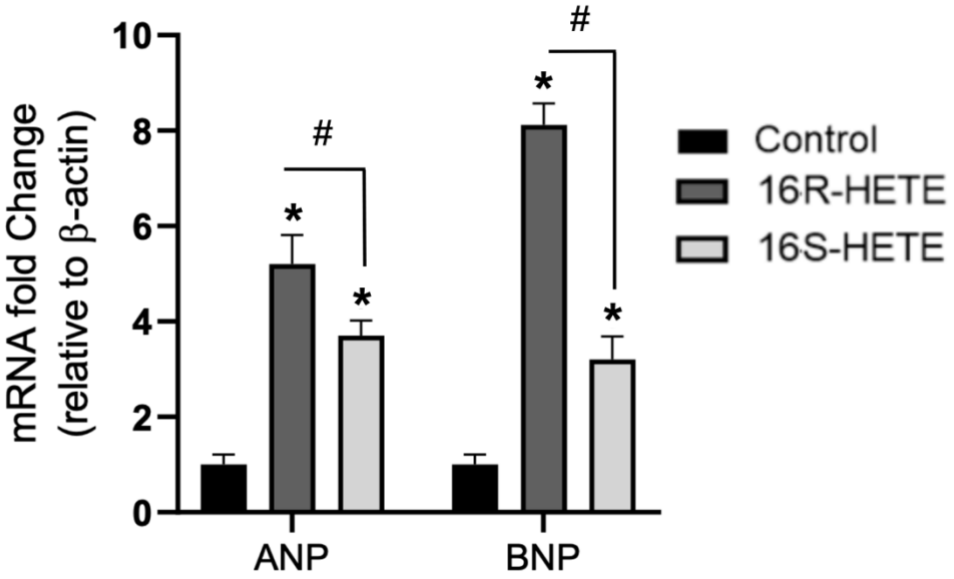

(B)

Figure 3.1.2. Effect of 16R-HETE and 16S-HETE on cellular hypertrophy in RL-14 cell lines. RL-14 cells were treated for 24 h with 20 μM; then, the mRNA levels α-MHC, β-MHC, ANP, and BNP were quantified using real time-PCR. The values represent the mean of fold change ± SEM (n = 6). +p<0.05 compared to control (concentration = 0 μM), and (#) $P < 0.05$, compared to respective 16R-HETE treatment.

3.1.3. Effect of 16R-HETE and 16S-HETE on cell surface area

The relative changes in cell surface area were assessed to verify that the modulation of hypertrophic markers in response to 16-HETE co-exposure is associated with cellular hypertrophy. It has been widely acknowledged that the change in cell surface area indicates cellular hypertrophy. For this reason, RL-14 cells were pretreated with 20 μM of both 16-HETE enantiomers. After that, the cell surface area was measured using the phase-contrast imaging taken with a Zeiss Axio Observer Z1 inverted microscope using an x20 objective lens.

Our results demonstrated a significant increase in cell surface area following the treatment of RL-14 cells with 20 μM 16-HETE enantiomers. This finding provided a piece of solid evidence that the rise in hypertrophic markers was associated with cellular hypertrophy. Interestingly, the degree of increase in cell surface area was parallel to the degree of hypertrophic markers modulation. In addition to that, the treatment with 16R-HETE caused a more dramatic increase compared to what 16S-HETE could bring about. As shown in Figure 3.1.3., after the treatment of RL-14 cells with 20 μM 16R-HETE, the cell surface area increased by 150% compared to control. Similarly, although to a lesser extent, the treatment with 16S-HETE promoted 95% enlargement of cell surface area.

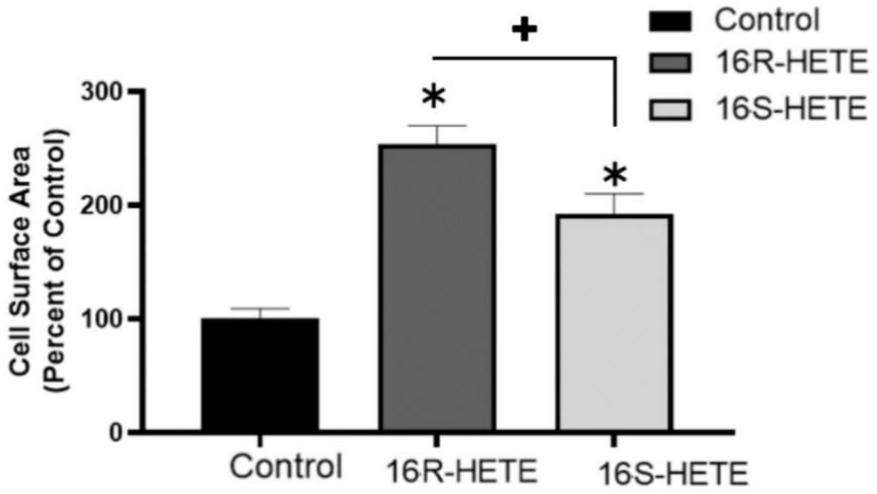

Figure 3.1.3. Effect of 16-HETE enantiomers on RL-14 cells surface area. RL-14 cells were treated with 20 μM for 24 h; then, the cell surface area was determined by phase-contrast imaging taken with a Zeiss Axio Observer Z1 inverted microscope using an x20 objective lens. The values represent the mean of fold change ± SEM (n = 6). *p<0.05 compared to control (concentration = 0 μM), and (+) $P < 0.05$, compared to respective 16R-HETE treatment.

3.1.4. Effect of 16-HETE enantiomers on *CYP1B1* gene expression in RL-14 cells.

To investigate the role of CYP1B1 in the induction of hypertrophic markers and cellular hypertrophy, the *CYP1B1* gene expression was evaluated. For this purpose, RL-14 cells were treated with various concentrations of 16-HETE enantiomers (2.5, 5, 10, and 20 μM). After that, the mRNA expression was quantified using real-time PCR as described in the material and methods. As expected, both enantiomers of 16-HETE modulated *CYP1B1* gene expression compared to control. However, the significant induction occurred at 20 μM concentration.

In parallel to the cellular hypertrophy, which is correlated to *CYP1B1* gene expression, 16R-HETE promoted more excellent induction than 16S-HETE. As shown in Figure 3.1.4., 16R-HETE significantly increases *CYP1B1* gene expressions by approximately five folds compared to control. Similarly, 16S-HETE also modulated it to a lesser degree than its enantiomer (4.21 folds), yet still significant compared to the control.

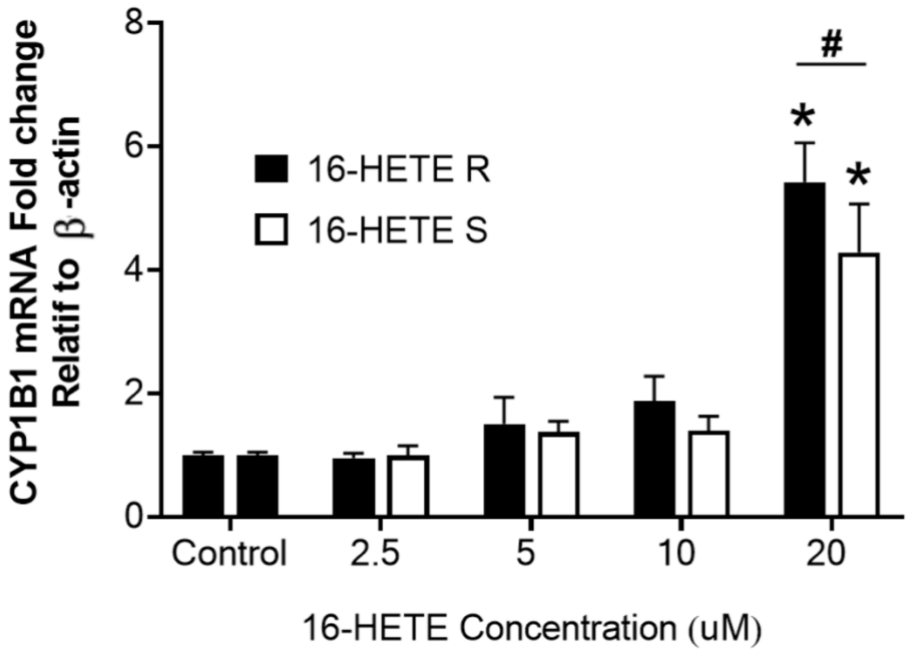

Figure 3.1.4. Effect of 16-HETE enantiomers on *CYP1B1* gene expressions. RL-14 cells were treated with 20 μM of 16-HETE enantiomers for 24 h. After that, CYP1B1 gene expression was quantified using real-time PCR and normalized to ß-actin. The values represent mean ± SEM (n=6). *P < 0.05 compared to control, and (#) *P* < 0.05, compared to respective 16R-HETE treatment.

3.1.5. Effect of 16-HETE enantiomers on CYP1B1 protein expression in RL-14 cells.

Since a remarkable induction of *CYP1B1* gene expression was observed following co-exposure of 16-HETE enantiomers in RL-14 cells, their effect on CYP1B1 expression was also evaluated. RL-14 cells were pretreated with 20 μM 16-HETE enantiomers. After that, Western Blot analysis was performed as described in the material and methods. Interestingly, CYP1B1 protein expression was in agreement with its gene expression modulation. Both 16-HETE enantiomers at the testing concentration significantly increased CYP1B1 protein expression compared to control.

Moreover, western blot analysis confirmed that 16R-HETE has a greater capacity in inducing CYP1B1 protein expression than its enantiomer: 16S-HETE. While 16R-HETE significantly approximately doubled CYP1B1 protein expression, 16S-HETE also significantly increased the protein expression up to 80 percent, compared to control (Figure 3.1.5).

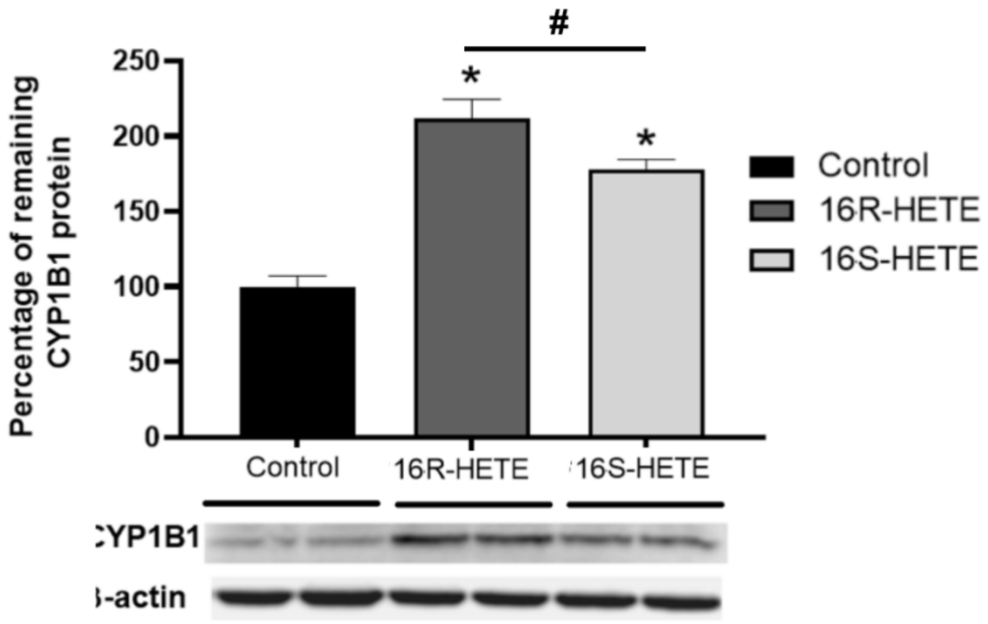

Figure 3.1.5. Effect of 16-HETE enantiomers on CYP1B1 protein expressions. RL-14 cells were treated with 20 μM of 16-HETE enantiomers for 24 h. After that, cell lysates were harvested, and CYP1B1 protein was determined using Western Blot analysis. To achieve optimum intensity, 75 ug of protein samples were used in the experiment. The graph represents the average optical density of bands from 6 different as a percent of control. *P < 0.05 compared to control, and (#) $P < 0.05$, compared to respective 16R-HETE treatment.

3.1.6. Effect of 16-HETE enantiomers on CYP1B1 enzyme activity

To examine whether the effect of 16-HETE enantiomers on *CYP1B1* gene expression was translated into catalytic activity, it is necessary to determine the impact of 16R-HETE and 16S-HETE on CYP1B1 enzyme activity. To do so, RL-14 cells were treated with 20 μM 16HETE enantiomers for 24 h. EROD, a substrate for the CYP1B1 enzyme was added accordingly, and the enzyme activity was measured as described in the material and methods. As shown in figure 3.1.6. below, both enantiomers of 16-HETE significantly increase CYP1B1 activity approximately two times compared to control.

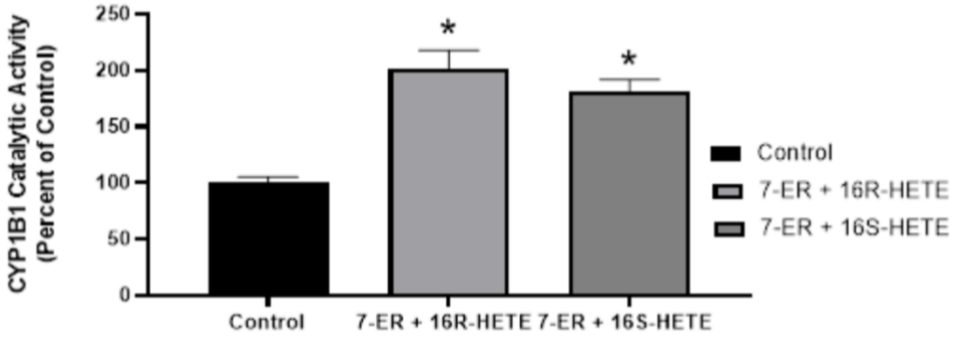

Figure 3.1.6. Effect of 16-HETE enantiomers on CYP1B1 activity. RL-14 cells were treated with 20 μM of 16-HETE enantiomers for 24 h. After that, the CYP1B1 catalytic activity level was determined by EROD assay. The values represent mean ± SEM (n=6). *P < 0.05 compared to control

3.1.7. Transcriptional regulation of *CYP1B*1 gene by 16-HETE enantiomers

A luciferase activity assay was conducted to determine whether an XRE-dependent mechanism mediates the observed effect of co-exposure of 16-HETE enantiomers on CYP1B1. For this purpose, recombinant HG2L7.5c1 human hepatoma cells stably transfected with an Ah receptor-responsive firefly luciferase reporter gene plasmid, pGudluc7.5 were utilized in the experiment. As depicted in Figure 3.1.7., luciferase activity results conveyed that both 16-HETE enantiomers at a concentration of 20 μM increase luciferase activity significantly by 110% and 100%, respectively, compared to control. Similarly, acting as a positive control, TCDD (1 nM) was capable of causing significant induction of luciferase activity by 750% compared to control.

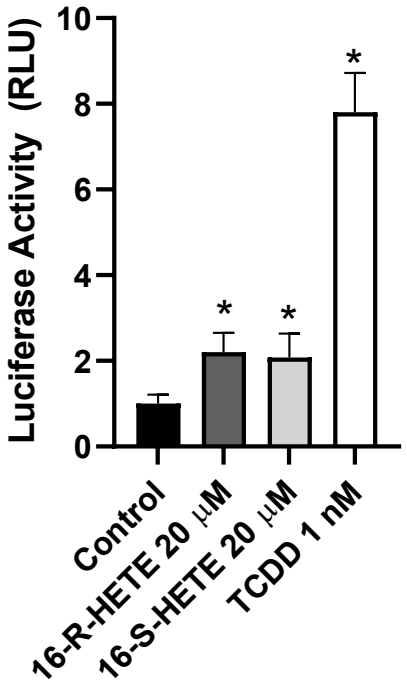

Figure 3.1.7. Effect of 16-HETE enantiomers on XRE-dependent luciferase activity. Recombinant HG2L7.5c1 human hepatoma cells stably transfected with an Ah receptor-responsive firefly luciferase reporter gene plasmid, pGudluc7.5 were used in the experiment. Cells were treated with vehicle, 16R-HETE (20 μM), 16S-HETE (20 μM), and TCDD (1 nM) for 24 h. After that, cells were lysed, and luciferase activity was measured according to the manufacturer's instructions. Luciferase activity is reported as a relative light unit (RLU). Values are presented as mean ± SEM (n=8). *P < 0.05 compared to control.

3.1.8. Transcriptional Induction of the *CYP1B1* gene by 16-HETE enantiomers

To investigate the mechanism involved in the induction of CYP1B1 mRNA by 16-HETE enantiomers in RL-14 cells, it is necessary to conduct an Act-D chase experiment. To perform this, before the treatment of 16-HETE enantiomers, RL-14 cells were treated with the transcription inhibitor, Act-D. If the stabilization of CYP1B1 mRNA were responsible for the effect caused by 16-HETE enantiomers, the effect of Act-D on the induced level of CYP1B1 mRNA would be abolished.

As shown in figure 3.1.8., co-exposure with Act-D completely inhibited the obtained CYP1B1 mRNA level induced by 16-HETE enantiomers. In other words, CYP1B1 mRNA induction by 16-HETE enantiomers required de novo RNA synthesis and suggested that the transcriptional mechanism was involved.

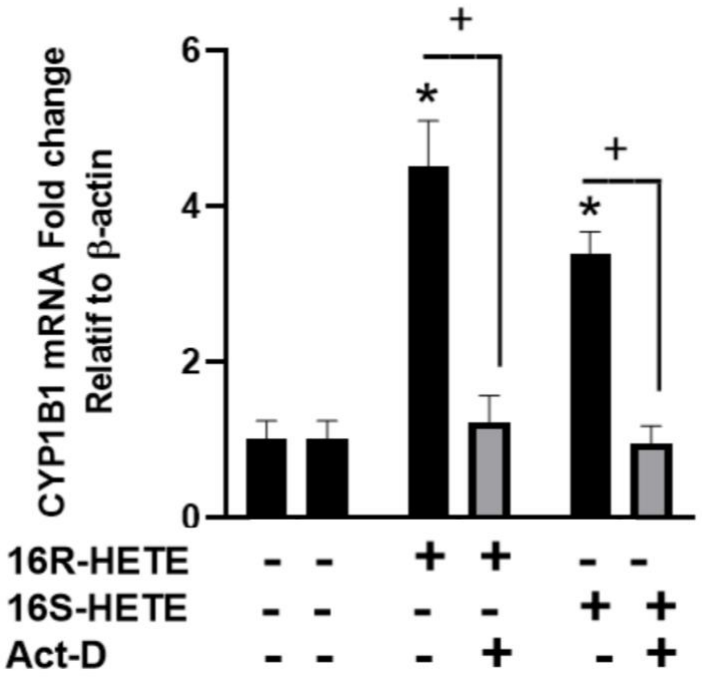

Figure 3.1.8. Transcriptional regulation of CYP1B1 by 16-HETE enantiomers. RL-14 cells were pretreated for 30 minutes with Act-D (5 µg/ml) prior to the treatment of 16R-HETE (20 µM) and 16S-HETE (20 µM for 24 h. After that, CYP1B1 mRNA gene expression was quantified using real-time PCR and normalized to ß-actin. Values are presented as mean ± SEM (n=6). *P < 0.05 compared to control, and (+) *P* < 0.05, compared to respective 16R-HETE treatment.

3.1.9. Post-transcriptional modification of CYP1B1 mRNA by 16-HETE enantiomers

The level of mRNA expression is a function of the transcriptions and eliminations rates through processing and degradation. Hence, it is critical to evaluate the effect of 16-HETE enantiomers on CYP1B1 mRNA transcript stability. If 16-HETE enantiomers stabilize CYP1B1 mRNA, there would be an increase in half-life. For this reason, the Act-D chase experiment was conducted. Our results showed that neither 16-HETE enantiomers nor TCDD significantly altered CYP1B1 mRNA stability on both conditions explored: constitutive and inducible levels.

As depicted by Figure 3.1.9., the vehicle-treated cells showed a CYP1B1 mRNA at the constitutive level with a half-life of (22.5 ± 0.32 h). Additionally, co-exposure of 16R-HETE and 16S-HETE did not alter CYP1B1 mRNA half-life that retained 50% of total mRNA at 24.23 ± 0.54 h and 23.65 ± 0.27 h, respectively. These findings indicate that the modulation of CYP1B1 mRNA transcripts in response to 16-HETE enantiomers was not due to an increase in its stability.

At the inducible level, shown in Figure 3.1.10., treatment of RL-14 cells with TCDD alone for 6 h resulted in a CYP1B1 mRNA half-life of 23.97 ± 0.41 h. While 16R-HETE retained half of the total mRNA at 25.7 ± 0.76 h, 16S-HETE could maintain CYP1B1 mRNA half-life at 25.3 ± 0.82 h. These values corroborate that both 16-HETE enantiomers did not significantly modify TCDD-induced CYP1B1 mRNA half-life.

(A)

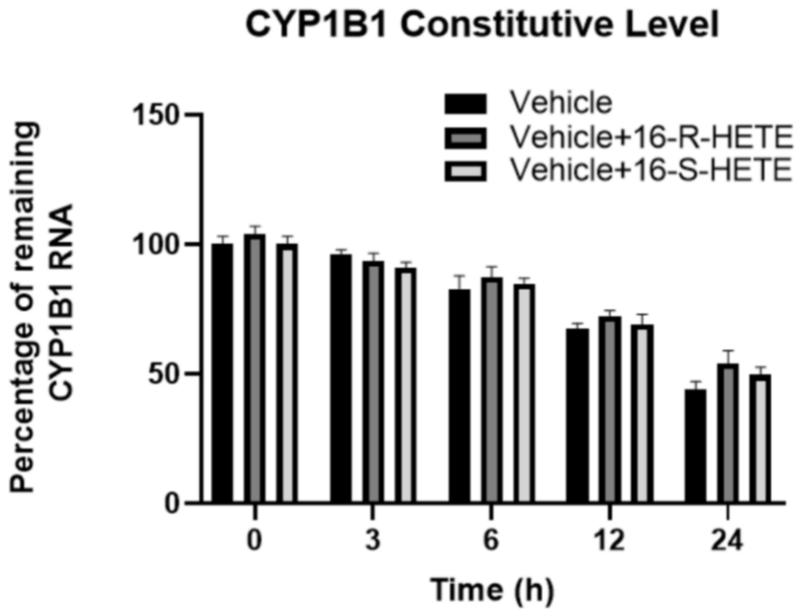

(B)

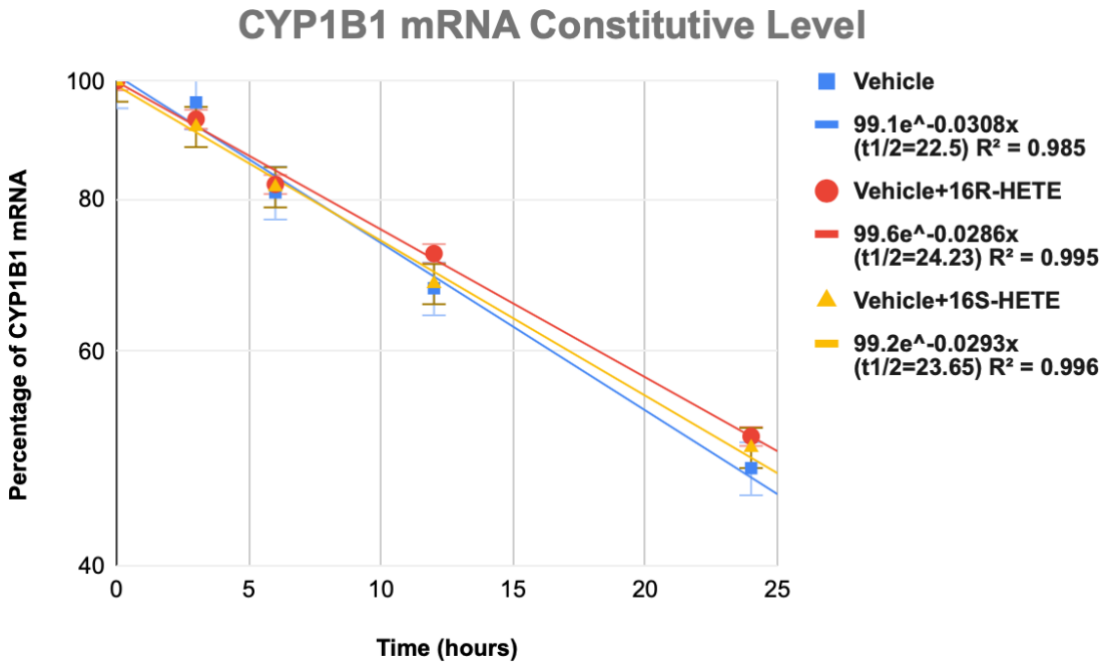

Figure 3.1.9. Effect of 16-HETE enantiomers on CYP1B1 mRNA stability using real-time PCR at the constitutive level. RL-14 cells were pretreated with Act-D (5 µg/ml), a transcription inhibitor, before the treatment of 16-HETE enantiomers. After that, total mRNA was extracted at 0, 1, 3, 6, and 12 h post-treatment. Total mRNA was extracted and

quantified using real-time PCR. mRNA decay curve was analyzed independently, and the half-life was estimated from the slope of a straight line fitted by linear regression analysis (r^2>0.85) to a semilog plot of mRNA amount to ensure the first kinetic order decay, set as a percent of treatment at the time= 0 h (maximum, 100%) level times. The half-lives obtained from three independent experiments were then used to calculate the mean half-life (mean ± SEM, n=3). *P 0.05 compared to vehicle-treated cells, *P < 0.05 compared to TCDD.

(A)

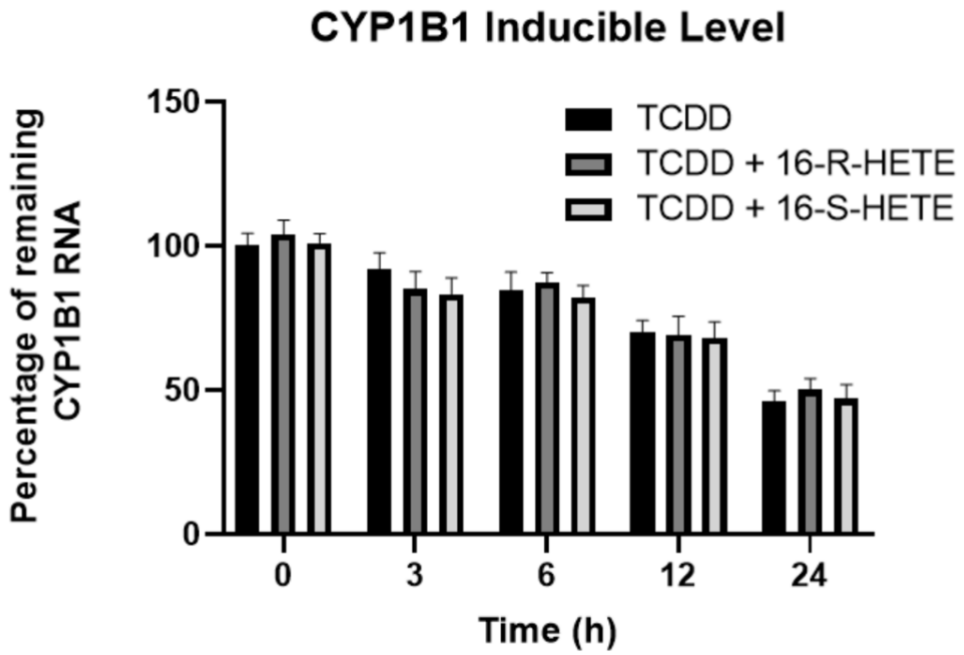

(B)

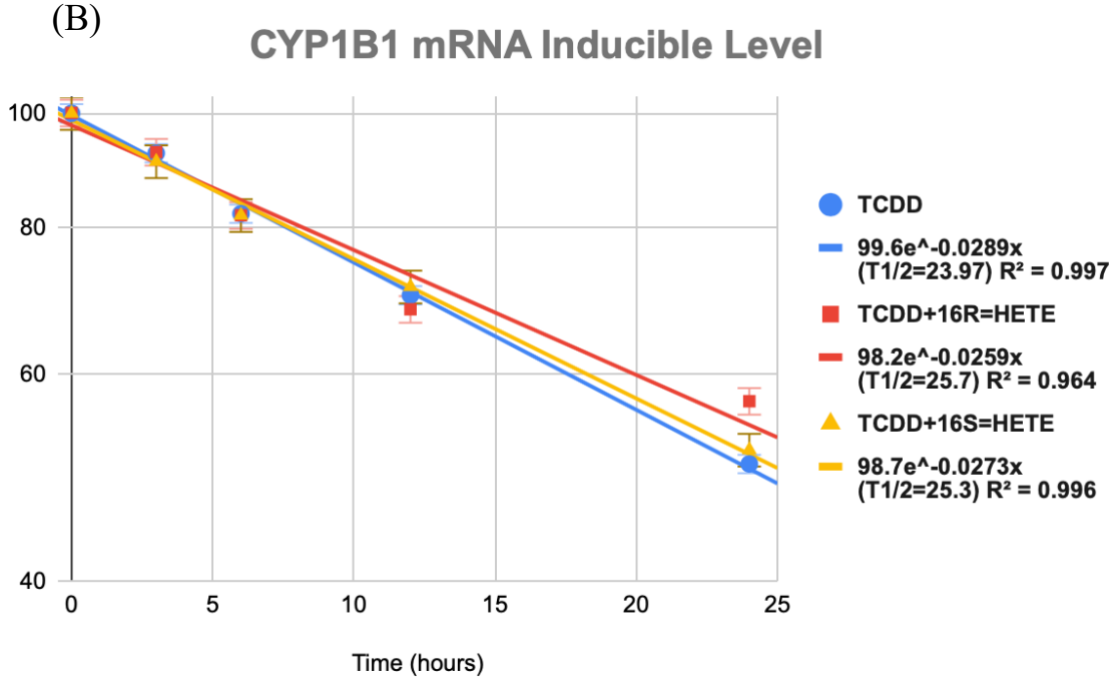

Figure 3.1.10. Effect of 16-HETE enantiomers on CYP1B1 mRNA stability using real-time PCR at inducible level. RL-14 cells were pretreated with TCDD for 6 h for the inducible level. After that, cells were washed and incubated with 5 µg/ml Act-D immediately

after treatment with 16-HETE enantiomers. After 0, 1, 3, 6, and 12 h post-treatment, total mRNA was extracted and quantified using real-time PCR. mRNA decay curve was analyzed independently, and the half-life was estimated from the slope of a straight line fitted by linear regression analysis (r^2>0.85) to a semilog plot of mRNA amount to ensure the first kinetic order decay, set as a percent of treatment at the time= 0 h (maximum, 100%) level times. The half-lives obtained from three independent experiments were then used to calculate the mean half-life (mean ± SEM, n=6)., *P < 0.05 compared to TCDD.

3.1.10. Post-translational modification of CYP1B1 protein by 16-HETE enantiomers

16-HETE enantiomers caused a significant increase CYP1B1 protein expression, which suggests that a post-translational mechanism might be involved. Hence, it is necessary to evaluate the stability of CYP1B1 protein through a CHX-chase experiment.

Figure 3.1.11.A. shows that TCDD retained 50% of the total CYP1B1 protein at 4.17 ± 0.29 h. Besides, the insignificant difference in CYP1B1 half-life was observed following the treatment of 16R-HETE alone for 24 h: 3.93 ± 0.23 h, compared to TCDD. Interestingly, 16R-HETE did not significantly affect the stability of TCDD-induced CYP1B1 protein, compared to what was obtained by TCDD, which degraded with a half-life of 4.77 ± 0.61 h.

A similar circumstance also occurred with the CYP1B1 protein stability in RL-14 cells treated with 16S-HETE. As shown in figure 3.1.10.B., the treatment of RL-14 cells with 16S-HETE for 24 h did not significantly alter the stability of CYP1B1 protein expression compared to TCDD, which was degraded with a half-life of 3.64 ± 0.57 h. Also, the treatment of RL-14 with this S enantiomer of 16-HETE did not modify the half-life of TCDD-induced CYP1B1 protein compared to TCDD alone, depicted by a half-life of 4.80 ± 0.63 h.

These findings indicate that the alteration in the stability of CYP1B1 protein expression following the treatment of 16 HETE enantiomers was not responsible for its modulation. Instead, it was solely due to an increase in its translation.

(A)

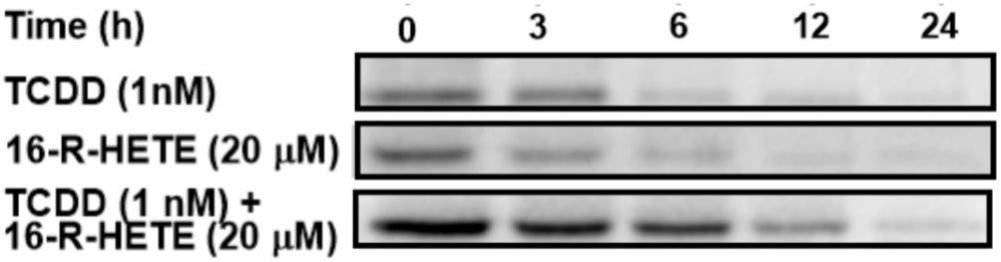
Time (h)
0
3
6
12
24
TCDD (1nM)
16-R-HETE (20 μM)
TCDD (1 nM) +
16-R-HETE (20 μM)

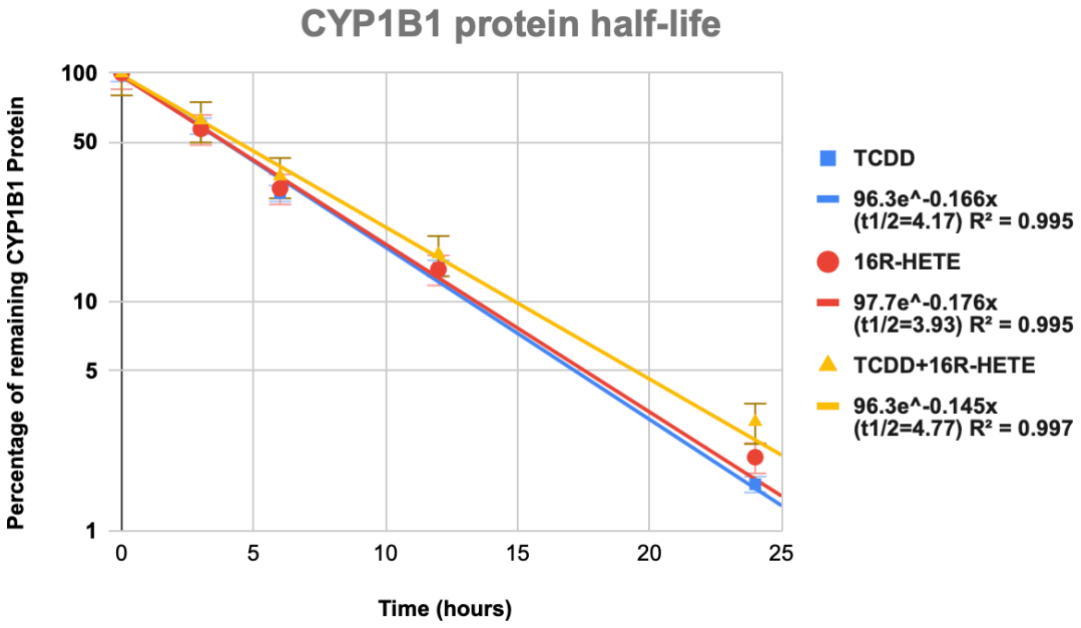
CYP1B1 protein half-life
Percentage of remaining CYP1B1 Protein
100
50
10
5
1
0
5
10
15
20
25
Time (hours)
TCDD
96.3e^-0.166x
(t1/2=4.17) R² = 0.995
16R-HETE
97.7e^-0.176x
(t1/2=3.93) R² = 0.995
TCDD+16R-HETE
96.3e^-0.145x
(t1/2=4.77) R² = 0.997

(B)

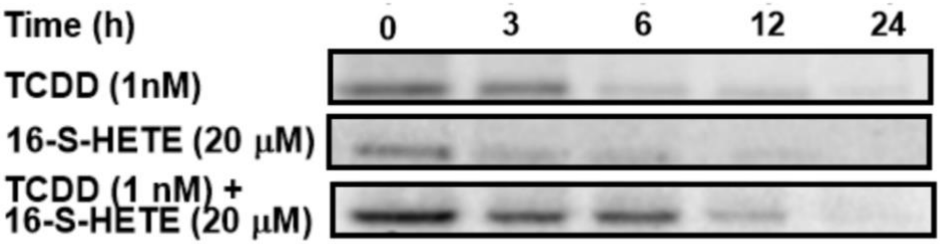

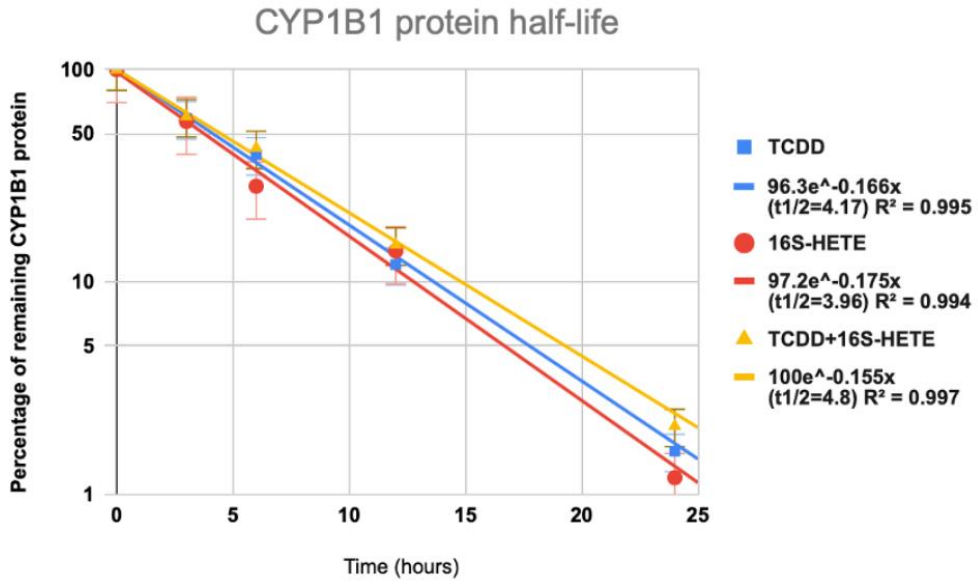

Figure 3.1.11. Effect of 16-HETE enantiomers on CYP1B1 protein. RL-14 cells were pretreated with TCDD 1 nM for 24 h. Afterward, they were washed and incubated in fresh media containing 20 μM 16 HETE enantiomers and 10 μg/ml protein translation inhibitor, cycloheximide (CHX). Furthermore, to determine CYP1B1 protein half-life in response to 16-HETE enantiomers, RL-14 cells were treated with 16-HETE enantiomers 20 μM for 24 h prior to treatment ten μ g/ml CHX. CYP1B1 protein was determined by Western blot analysis as described in Materials and methods. The intensities of CYP1B1 protein bands were normalized to β-Actin signals, which were used as loading controls. All protein decay curves were analyzed individually. The half-life was estimated from the slope of a straight line fitted by linear regression analysis ($r^2 \geq 0.85$) to a semilog plot of protein amount, expressed as a percentage of treatment at time=0 h (maximum, 100%) level versus time. The

half-lives obtained from three independent experiments were then used to calculate the mean half-life (mean±S.E.M., n=3). +Pb 0.05 compared to TCDD.

3. 2. 16-HETE enantiomers alter human CYP1B1 and CYP1A2 through an allosteric mechanism.

3.2.1. 16-HETE enantiomers increase human CYP1B1 enzyme through allosteric activation.

An increase in CYP1B1 enzyme activity will manifest a higher risk of cardiac hypertrophy development. Hence, we examined the capacity of 16-HETE enantiomers to increase the catalytic activity of human recombinant CYP1B1 based on our previous finding that these CYP-mediated metabolites increase CYP1B1 catalytic activity in the human fetal ventricular cardiomyocytes, RL-14 cells. For this purpose, the modulation properties of 16-HETE enantiomers on CYP1B1 were evaluated using CYP1B1 substrate, 7-ethoxyresorufin (7-ER), which is metabolized by the enzyme via an oxidative reaction to form a resorufin. In this regard, CYP1B1 facilitated an O-dealkylation of 7-ER. Therefore, the catalytic activity of human recombinant CYP1B1 was determined by measuring the EROD reaction rate over time. If a velocity rate of EROD is observed, represented in an increase of the resorufin formation, it means that the activity of human recombinant CYP1B1 increased.

The modulatory properties of 16-HETE enantiomers on human recombinant CYP1B1 were studied. Before the experiment, the experimental conditions such as 7-ER concentration, recombinant enzyme concentrations, and incubation time were all optimized before adding either 16R-HETE or 16S-HETE. Based on the non-linear regression analysis and fitting to the simple Michaelis Menten equation, it was observed that both 16-HETE enantiomers increase the activity of CYP1B1. However, the curve did not fit well to the Michaelis Menten. Rather, the model that provided a much better fit to the data was the sigmoidal Michaelis-Menten equation. This suggested that there is allosteric cooperativity involved in the mechanism in which 16-HETE enantiomers increase human recombinant CYP1B1. As shown in Figures 1.A. and 1.B., the maximum EROD activity (Vmax) in

control containing 0.1% dimethyl sulfoxide was 10.021 pmol resorufin/pmol P450 per minute (R2 = 0.9862) (Table1). Initially, a significant increase in CYP1B1 activity was increased during the co-incubation of either 5 nM concentration of 16R-HETE or 16S-HETE on different concentrations of 7-ER (0-100 nM), encouraging us to utilize various concentrations of both 16-HETE enantiomers.

As shown in Figures 3.2.1. and 3.2.2., the maximum EROD activity (Vmax) in control containing 0.1% dimethyl sulfoxide was 10.021 pmol resorufin/pmol P450 per minute (R2 = 0.9862) (Table1). Initially, a significant increase in CYP1B1 activity was observed during the co-incubation of either 10 nM 16R-HETE or 16S-HETE on concentrations of 7-ER (0-100 nM). Then, we tested various concentrations of both 16-HETE enantiomers to see the degree of induction. As expected, more prominent resorufin formation rates were observed as more 16-HETE enantiomers were available in the environment, confirming that allosteric activation was involved. In addition to that, the maximum velocity and Km of CYP1B1 is more significant than what could be induced by 16S-HETE. This result indicates that 16R-HETE promoted greater activation than its enantiomer: 16S-HETE.

As shown in table 3.2.1, the Vmax and Km of CYP1B1 increase significantly as more 16-HETE enantiomers were available in the environment. Consequently, the CL_{int} increases significantly in the presence of 16R-HETE or 16S-HETE.

(A)

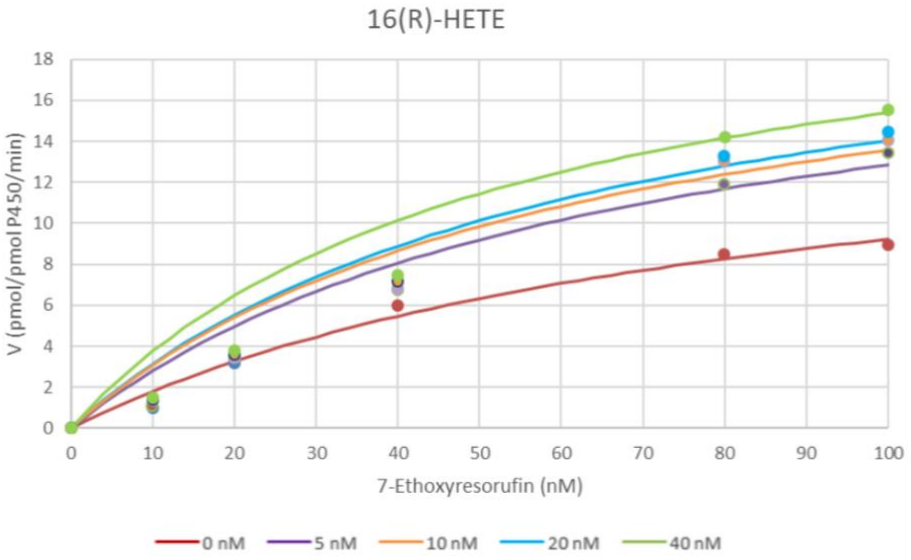

(B)

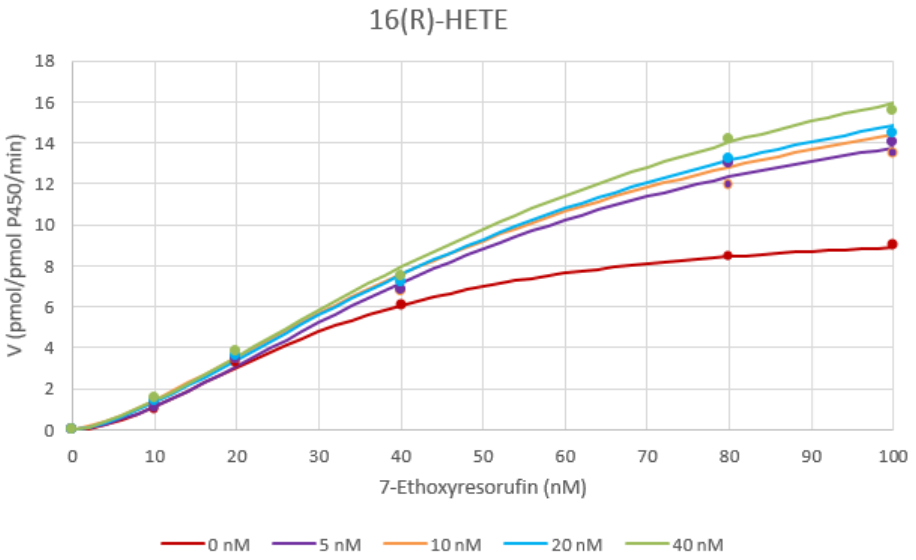

Figure 3.2.1. 16R-HETE increase human CYP1B1 enzyme through allosteric activation. In 96-well solid black polystyrene plates, the reaction mixture containing buffer and 1 pmol of human CYP1A1 was incubated with 10-200 nM of 7-ER. Into the mixture, 0, 5, 10, 20, or 40 nM of 16R-HETE were added. After that, 100 ul of 2mM NADPH was added to initiate the reaction. The fluorescent signal related to resorufin formation was measured every min (excitation and emission wavelengths of 550 and 585 nm, respectively, for 30 min at 37°C using BioTek Synergy H1Hybrid. The quantity of formed resorufin was measured

by constructing a standard curve of 0-200 nM resorufin dissolved in the same incubation buffer. (A) Michaelis Menten model (B) Hill coefficient model.

(A)

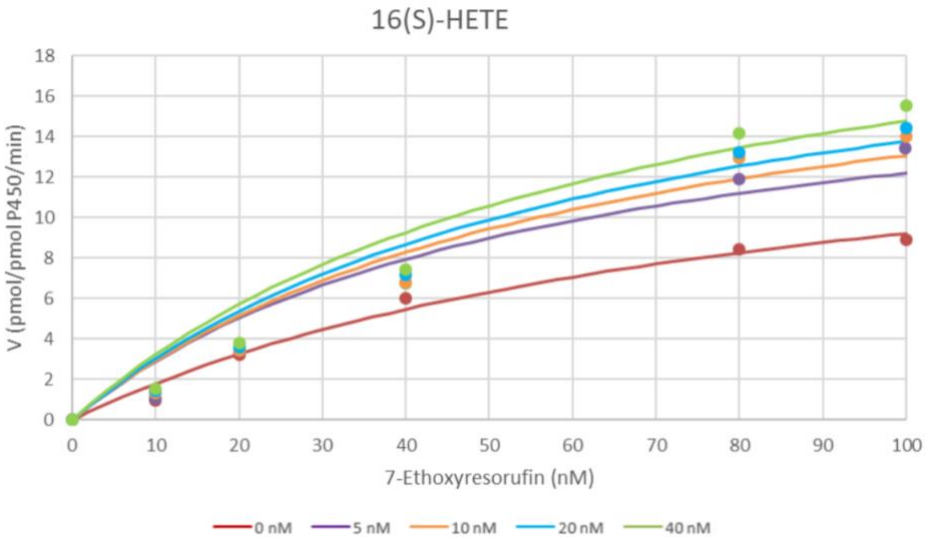

(B)

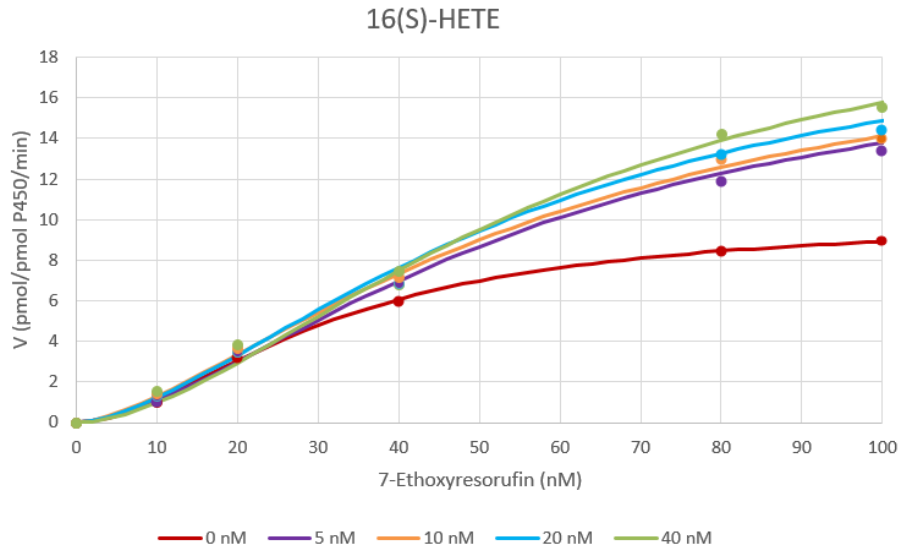

Figure 3.2.2. 16S-HETE increase human CYP1B1 enzyme through allosteric activation. In 96-well solid black polystyrene plates, the reaction mixture containing buffer and 1 pmol of human CYP1B1 was incubated with 10-200 nM of 7-ER. Into the mixture, 0, 5, 10, 20, or 40 nM of 16S-HETE were added. After that, 100 ul of 2mM NADPH was added to initiate the reaction. The fluorescent signal related to resorufin formation was measured every min (excitation and emission wavelengths of 550 and 585 nm, respectively, for 30 min at 37°C using BioTek Synergy H1Hybrid. The quantity of formed resorufin was measured by constructing a standard curve of 0-200 nM resorufin dissolved in the same incubation buffer. (A) Michaelis Menten model (B) Hill coefficient model.

Table 3.2.1. The kinetic parameters of resorufin formation by human recombinant CYP1B1 using Hill equation.

The mean values and standard error of kinetic parameters of resorufin formation by human recombinant CYP1A2, in the absence and presence, in the absence and presence of 16-HETE enantiomers. Results are presented as mean and SD, based on at least 3 individual experiments. Km, and Vmax, and CL_{int} ± SD were determined by Enzyme Kinetics module from GraphPad Prism, version 5.01, and Microsoft Excel Solver.

Kinetics of resorufin formation				
16R-HETE Concentration	**Vmax (pmol/pmol P450/min)**	**Km (nM)**	**CLint (mL/pmol P450/min)**	**n (Hill Coefficient)**
0 nM	10.0 ± 1.09	31.5 ± 3.22	0.31 ± 0.01	1.84 ± 0.03
5 nM	18.7 ± 0.82*	53.7 ± 2.71*	0.35 ± 0.01*	1.66 ± 0.04
10 nM	21.1 ± 0.44*	59.2 ± 3.01*	0.36 ± 0.01*	1.43 ± 0.03*
20 nM	21.8 ± 0.62*	60.6 ± 4.22*	0.36 ± 0.03*	1.50 ± 0.03*
40 nM	24.5 ± 1.03*	65.7 ± 3.51*	0.37 ± 0.02*	1.51 ± 0.02*
16R-HETE Concentration	**Vmax (pmol/pmol P450/min)**	**Km (nM)**	**CLint (mL/pmol P450/min)**	**n (Hill Coefficient)**
0 nM	10.0 ± 1.09	31.5 ± 3.22	0.31 ± 0.01	1.84 ± 0.03
5 nM	18.3 ± 1.03*	55.3 ± 2.80*	0.32 ± 0.02	1.67 ± 0.03
10 nM	20.3 ± 0.72*	58.0 ± 2.83*	0.34 ± 0.01*	1.55 ± 0.01*
20 nM	20.6 ± 0.48*	60.6 ± 3.51*	0.35 ± 0.02*	1.59± 0.02*
40 nM	21.9 ± 0.51*	58.2 ± 4.01*	0.36 ± 0.03*	1.71 ± 0.04

Data are presented as mean ± SD (n=6). *Vmax*, maximum velocity; *Km*, the concentration at which the rate is one-half of the Vmax; Clint, intrinsic clearance; and n, Hill coefficient. Groups showing * symbol indicate a statistically significant difference ($p<0.05$) from control group (0 nM 16-HETE enantiomers).

3.2.2. 16-HETE enantiomers inhibit human CYP1A2 enzyme through allosteric inhibition

16-HETE enantiomers could increase human recombinant CYP1B1 activity is a peculiar phenomenon. Hence, to explore the modulatory properties of 16-HETE enantiomers more profoundly, we testified the effect of 16R-HETE and 16S-HETE on different human recombinant CYP enzymes. Among CYP members, it has been widely acknowledged that, besides CYP1B1, CYP1A2 was also regulated by AhR. Based on preliminary information, we evaluated the effect of 16-HETE enantiomers on the modulatory properties of CYP1A2. For this purpose, the modulation properties of 16-HETE enantiomers on CYP1A2 were assessed using the CYP1A2 substrate, methoxyresorufin (MR). Like 7-ER, MR is metabolized via an O-dealkylation reaction by CYP1A2 to form a resorufin. Therefore, the catalytic activity of human recombinant CYP1A2 was determined by measuring the MROD reaction rate over time. If there is a change in the MROD velocity rate, it indicates that 16-HETE enantiomers could alter the activity of various human recombinant enzymes.

The modulatory properties of 16R-HETE and 16S-HETE on human recombinant CYP1A2 were studied. Before, the experimental conditions such as 7-ER and recombinant enzyme concentrations used in the experiment and incubation time were optimized prior to adding 16-HETE enantiomers. The data was analyzed using the non-linear regression analysis and fitted to the Michaelis Menten equation; however, the curve did not fit the Michaelis Menten. Hence, Microsoft Excel Solver was used to define the corresponding hill coefficient. Based on this software, we observe that the sigmoidal type was the most probable binding mode. This sigmoidal curve indicated that allosteric cooperativity was involved in

the mechanism in which 16-HETE enantiomers inhibit human recombinant CYP1A2. Moreover, it is contradictory to what we observed in the human recombinant CYP1B1.

Figure 3.2.3. and 3.2.4. show that both 16-HETE enantiomers inhibit human recombinant CYP1A2. The maximum MROD activity (Vmax) in control containing 0.1% dimethyl sulfoxide was 19.939 pmol resorufin/pmol P450 per min (R2 = 0.987) (Table2). Interestingly, a significant inhibition in CYP1A2 activity was observed during the co-incubation of 10 nM 16R-HETE enantiomers on different concentrations of 7-MR (0-100 nM). This finding prompted us to test various concentrations of both 16R-HETE and 16S-HETE. Interestingly, more prominent inhibitions of CYP1A2 activity were observed as more 16-HETE enantiomers were available in the environment, indicating an allosteric inhibition was involved. Furthermore, as shown in table 3.2.2, Vmax and Km of CYP1A2 decline significantly as more 16-HETE enantiomers added to the mixture. As a result, the CL_{int} decreases significantly in the presence of 16 HETE enantiomers.

(A)

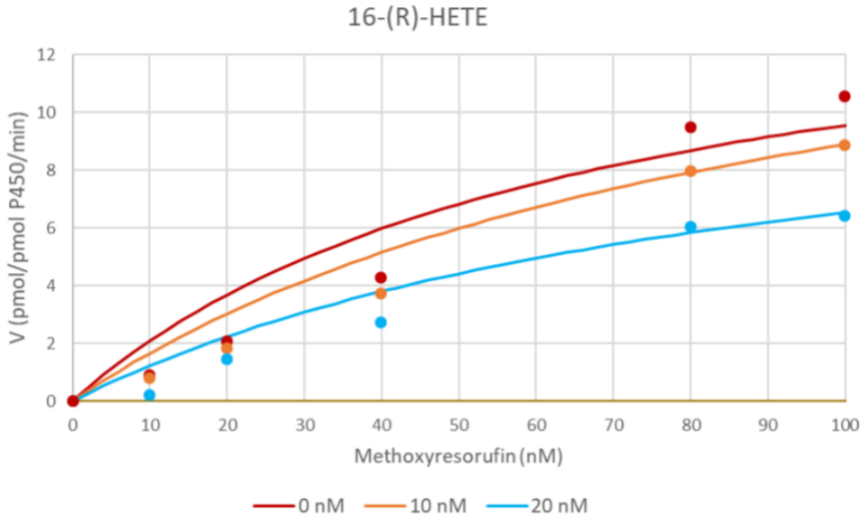

(B)

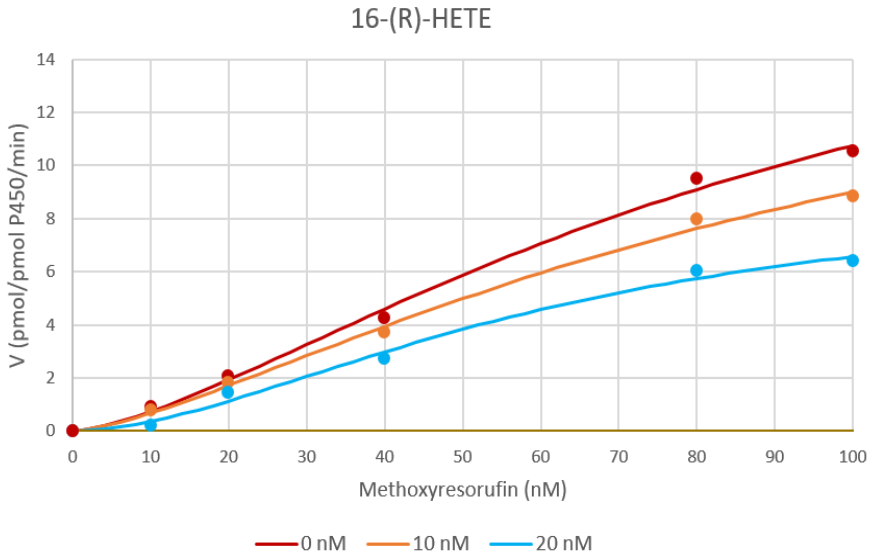

Figure 3.2.3. 16R-HETE inhibit human CYP1A2 enzyme through allosteric inhibition. In 96-well solid black polystyrene plates, the reaction mixture containing buffer and 1 pmol of human CYP1A2 was incubated with 10-200 nM of 7-ER. Into the mixture, 0, 5, 10, 20, or 40 nM of 16R-HETE were added. After that, 100 ul of 2mM NADPH was added to initiate the reaction. The fluorescent signal related to resorufin formation was measured every min (excitation and emission wavelengths of 550 and 585 nm, respectively, for 30 min at 37°C using BioTek Synergy H1 Hybrid. The quantity of formed resorufin was measured by

constructing a standard curve of 0-200 nM resorufin dissolved in the same incubation buffer. (A) Michaelis Menten model (B) Hill coefficient model.

(A)

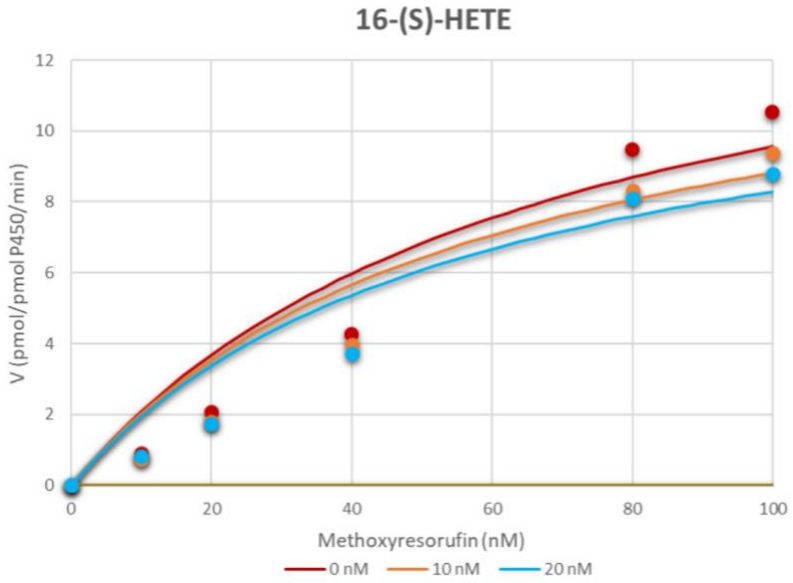

(B)

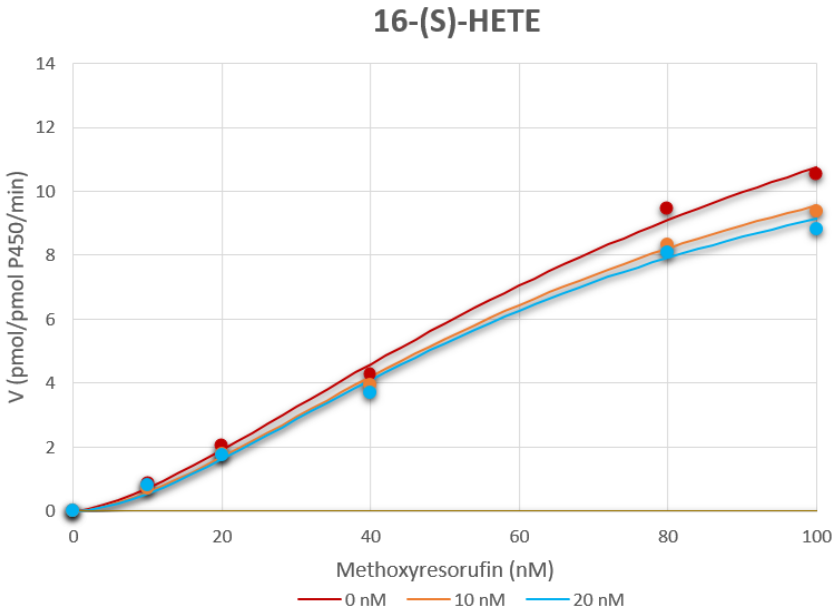

Figure 3.2.4. 16S-HETE inhibit human CYP1A2 enzyme through allosteric inhibition. In 96-well solid black polystyrene plates, the reaction mixture containing buffer and 1 pmol

of human CYP1A2 was incubated with 10-200 nM of 7-ER. Into the mixture, 0, 5, 10, 20, or 40 nM of 16S-HETE were added. After that, 100 ul of 2mM NADPH was added to initiate the reaction. The fluorescent signal related to resorufin formation was measured every minute (excitation and emission wavelengths of 550 and 585 nm, respectively, for 30 minutes at 37°C using BioTek Synergy H1 Hybrid. The quantity of formed resorufin was measured by constructing a standard curve of 0-200 nM resorufin dissolved in the same incubation buffer (A) Michaelis Menten model (B) Hill coefficient model.

Table 3.2.2. The kinetic parameters of resorufin formation by human recombinant CYP1A2. The mean values and standard error of kinetic parameters of resorufin formation by human recombinant CYP1A2, in the absence and presence, in the absence and presence of 16-HETE enantiomers. Results are presented as mean and SD, based on at least 3 individual experiments. Km, and Vmax, and Clint ± SD were determined by Enzyme Kinetics module from GraphPad Prism, version 5.01, and Microsoft Excel Solver.

Kinetics of resorufin formation				
16R-HETE Concentration	**Vmax (pmol/pmol P450/min)**	**Km (nM)**	**CLint (mL/pmol P450/min)**	**n (Hill Coefficient)**
0 nM	19.9 ± 0.61	89.9 ± 3.12	0.22 ± 0.02	1.49 ± 0.03
10 nM	17.3 ± 0.48*	86.5 ± 2.81	0.21 ± 0.01	1.75 ± 0.01*
20 nM	9.30 ± 0.42*	61.5 ± 3.52*	0.15 ± 0.03*	1.73 ± 0.03*
Kinetics of resorufin formation				
16S-HETE ConcentrationS	**Vmax (pmol/pmol P450/min)**	**Km (nM)**	**CLint (mL/pmol P450/min)**	**n (Hill Coefficient)**
0 nM	19.9 ± 0.61	89.9 ± 3.12	0.22 ± 0.02	1.49 ± 0.03
10 nM	17.2 ± 0.88*	73.8 ± 3.22*	0.21 ± 0.02	1.58 ± 0.03
20 nM	13.9 ± 0.73*	67.2 ± 4.31*	0.19 ± 0.01*	1.66 ± 0.02*

Data are presented as mean ± SD (n=6). *Vmax*, maximum velocity; *Km*, the concentration at which the rate is one-half of the Vmax; Clint, intrinsic clearance; and n, Hill coefficient. Groups showing * symbol indicate a statistically significant difference ($p<0.05$) from control group (0 nM 16-HETE enantiomers).

3.2.3. 16-HETE increase EROD activity; yet, inhibit MROD activity in human liver microsomes

In reality, CYP1B1 and CYP1A2 do not stand alone; instead, they are parts of human liver microsomes. Hence, to further confirm the results obtained from the recombinant enzymes, we explored the possible allosteric modulation of 16-HETE enantiomers on the catalytic activity of EROD and MROD, using human liver microsomes that were polled from 25 individuals. Fixed concentrations of the substrate were used in each assay with varying concentrations of either 16R-HETE or 19-S-HETE enantiomers (0, 20, 40, 80, 160, and 200 nM).

Our results showed that an increase in resorufin formation rate appeared as the concentrations of 16-HETE enantiomers increased (Fig. 3.2.5.A). During the co-incubation of the human liver microsome with a range of 16R-HETE concentrations, the EROD rate increased gradually compared to the control group. The significant increase in CYP1B1 catalyzed EROD activity was achieved with 200 nM of 16R- and 16S-HETE that could increase resorufin formation rate up to 127.2% and 116.1% respectively.

On the other hand, as expected, there is a significant decrease in MROD activity after co-exposure with 16-HETE enantiomers in human liver microsomes. (Fig. 3.2.5.B). During the co-incubation of the human liver microsome with a range of 16R-HETE concentrations, the EROD rate increased gradually compared to the control group. 16R- and 16S-HETE 200 nM could inhibit 42.3% and 37% of CYP1A2 catalyzed MROD activity compared to when there is no 16-HETE enantiomers in the environment. 16R-HETE and 16S-HETE have IC_{50} values of 289.6 and 245.2 nM, respectively.

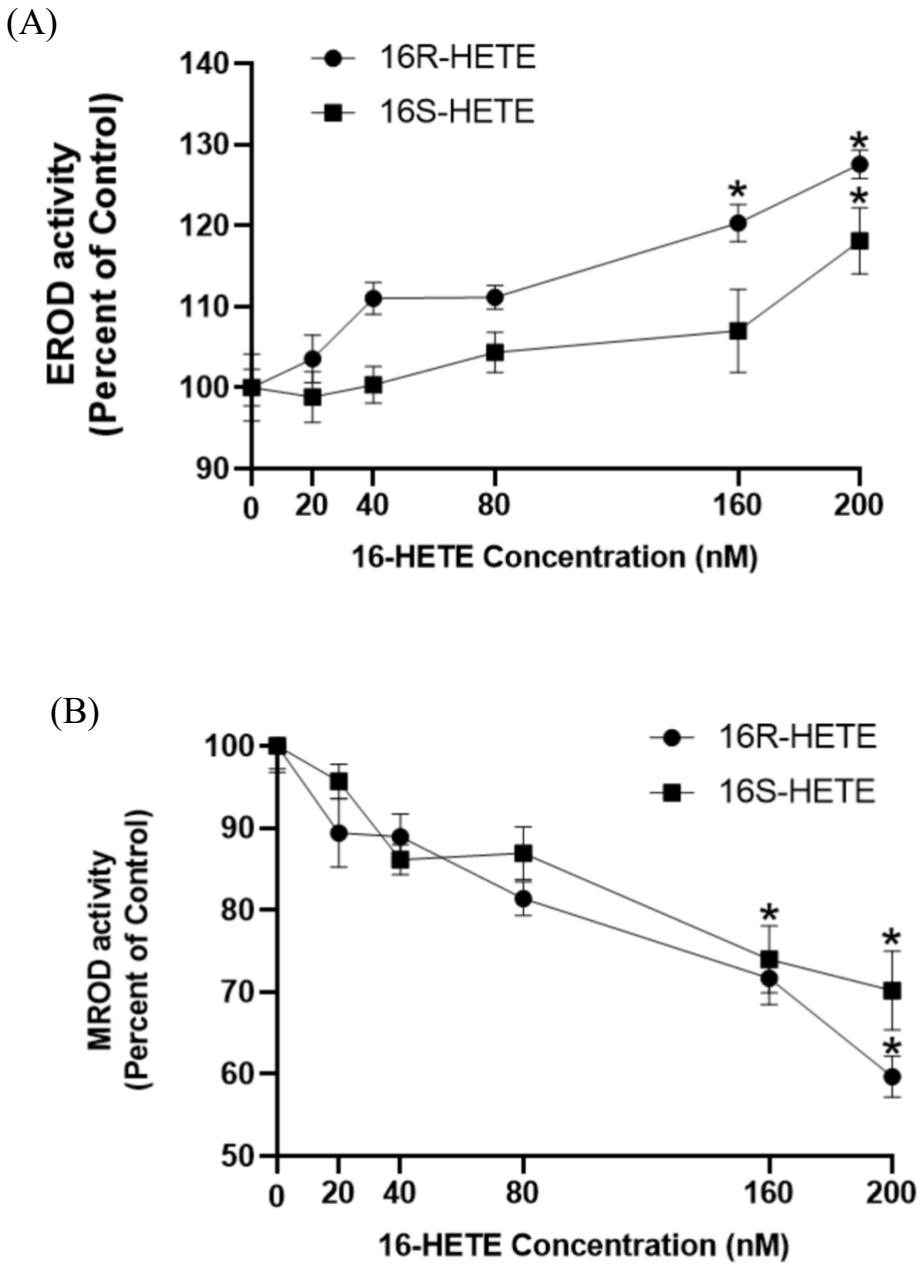

Figure 3.2.5. 16-HETE enantiomers alter human CYP1B1 and CYP1A2 mediated by human liver microsomes. Human liver microsomes were used in a concentration of 0.2 mg/ml in the absence and presence of varying concentrations of 16-HETE enantiomers. In

addition, 2 μM of 7-ER for EROD assay or 5 μM of 7-MR for MROD assay were used as substrates. The reaction was initiated by adding 100 μL of 2 mM NADPH, the fluorescent signal related to the formation of resorufin was measured. The results are presented as the means of six independent experiments ± SEM.

3.2.4. CYP1B1 has more than one probable binding sites.

Available crystal structures of the CYP1B1 enzyme (table 3.3.1) were evaluated using a homology modeling study to explore this possibility. Figure 3.2.4. shows the catalytic domain of CYP1B1, while figure 3.2.5. shows that CYP1B1 has at least 12 probable pockets from this computational approach. One orthosteric site in the center of the enzyme and other possible allosteric sites far away from the center is located among these pockets.

Table 3.1.1. CYP1B1 sequence adopted from UniprotKB entry number Q16678

```
    10         20         30         40         50
MGTSLSPNDP WPLNPLSIQQ TTLLLLLSVL ATVHVGQRLL RQRRRQLRSA
        60         70         80         90        100
PPGPFAWPLI GNAAAVGQAA HLSFARLARR YGDVFQIRLG SCPIVVLNGE
       110        120        130        140        150
RAIHQALVQQ GSAFADRPAF ASFRVVSGGR SMAFGHYSEH WKVQRRAAHS
       160        170        180        190        200
MMRNFFTRQP RSRQVLEGHV LSEARELVAL LVRGSADGAF LDPRPLTVVA
       210        220        230        240        250
VANVMSAVCF GCRYSHDDPE FRELLSHNEE FGRTVGAGSL VDVMPWLQYF
       260        270        280        290        300
PNPVRTVFRE FEQLNRNFSN FILDKFLRHC ESLRPGAAPR DMMDAFILSA
       310        320        330        340        350
EKKAAGDSHG GGARLDLENV PATITDIFGA SQDTLSTALQ WLLLLFTRYP
       360        370        380        390        400
DVQTRVQAEL DQVVGRDRLP CMGDQPNLPY VLAFLYEAMR FSSFVPVTIP
       410        420        430        440        450
HATTANTSVL GYHIPKDTVV FVNQWSVNHD PLKWPNPENF DPARFLDKDG
       460        470        480        490        500
LINKDLTSRV MIFSVGKRRC IGEELSKMQL FLFISILAHQ CDFRANPNEP
         510        520        530        540
   AKMNFSYGLT IKPKSFKVNV TLRESMELLD SAVQNLQAKE TCQ
```

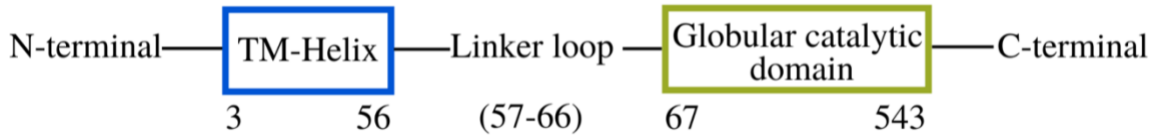

Figure 3.2.6. Catalytic domain of CYP1B1. Human CYP1B1 is a protein of 543 amino acids, of which 53 are part of an N-terminal membrane-binding domain, 10 are located in a proline-rich hinge region, and 476 make up the globular catalytic domain (Nishida et al., 2013).

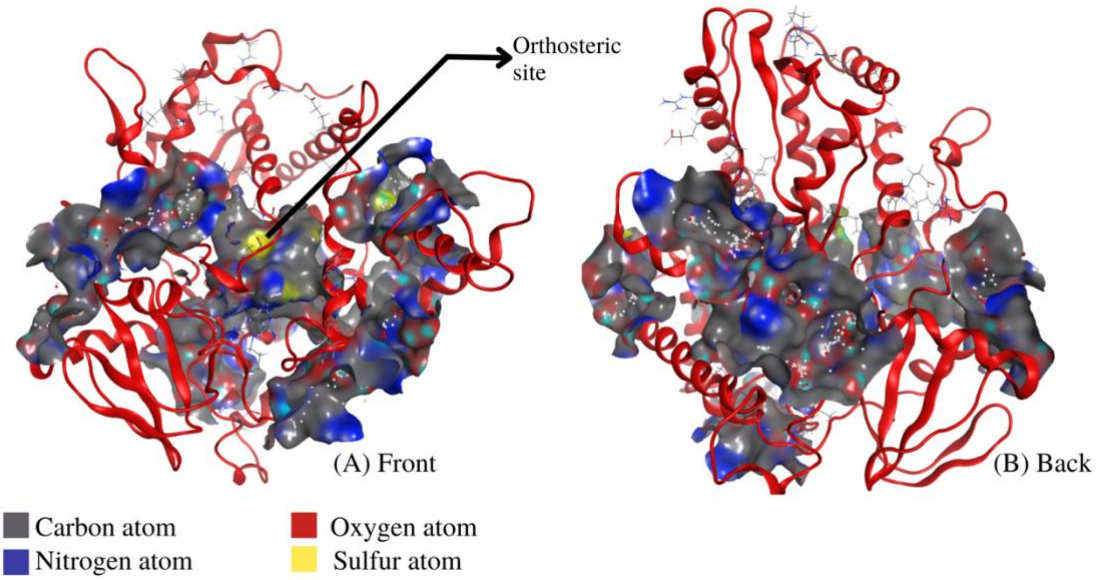

Figure 3.2.7. Crystal structure of CYP1B1. CYP1B1 has at least 11 probable binding sites that can serve as an allosteric site in addition to the orthosteric binding site at the center of the enzyme.

3.2.5. Illustration of Allosteric modulation by 16-HETE enantiomers.

Figure 3.2.5. shows an illustration of how 16-HETE enantiomers produce their effect on human recombinant CYP1B1 and CYP1A2. In the first illustration, 16-HETE enantiomers might bind to an allosteric binding site of CYP1B1, change the conformation of the orthosteric binding sites, and stabilize its resting state, allowing more substrates to interact in that area and increase the EROD activity rate. This type of binding is widely called allosteric activation. On the contrary, the binding of 16-HETE enantiomers to CYP1A2 allosteric binding sites stabilizes the tight state of the orthosteric site, preventing more substrate from binding to it and decreasing the MROD activity. This type of binding is called allosteric inhibition.

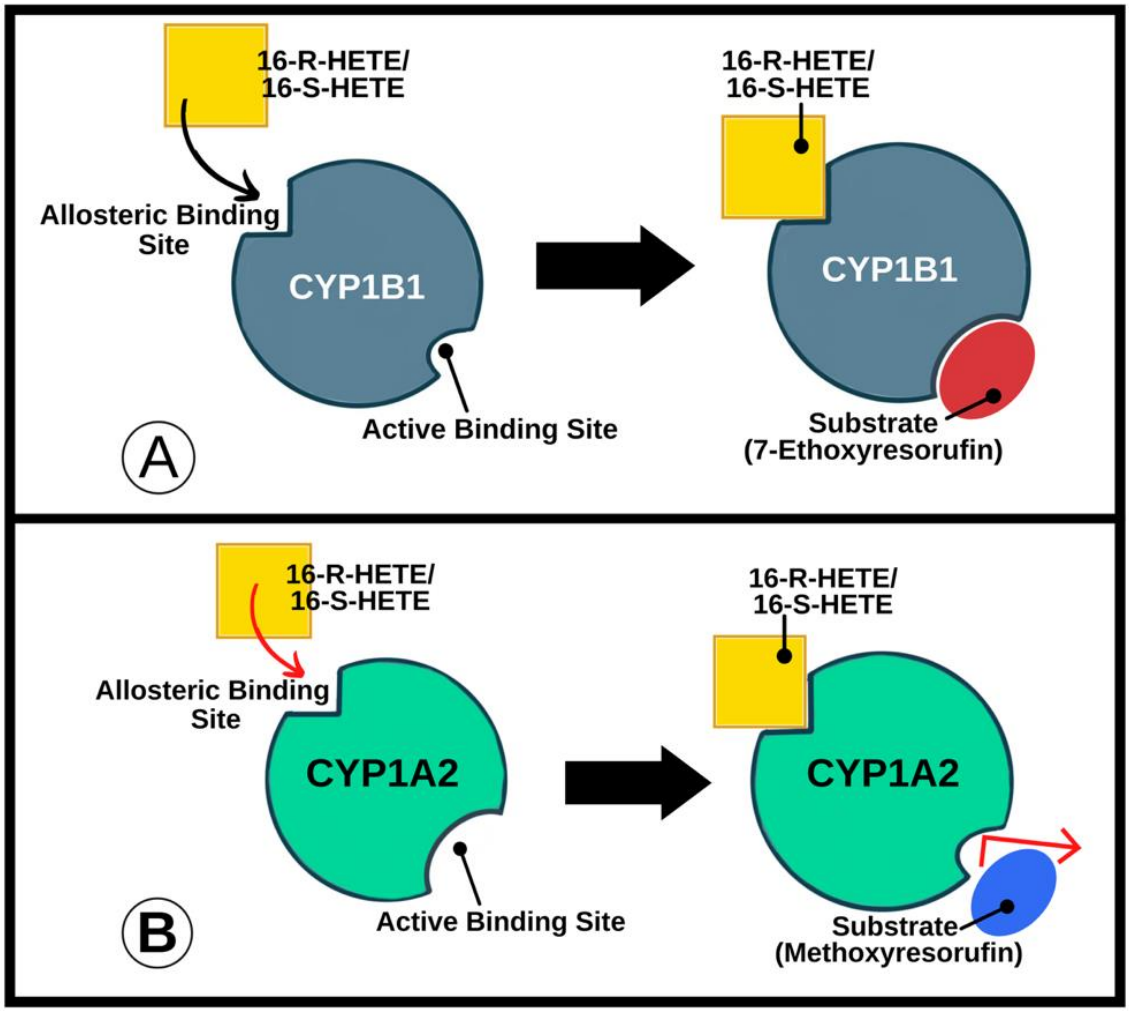

Figure 3.2.8. Illustration of Allosteric modulation by 16-HETE enantiomers. 16-HETE enantiomers act as an allosteric activation on CYP1B1 (A); yet, as an allosteric inhibition on CYP1A2.

Chapter 4: Discussion

The role of CYP enzymes and their AA metabolites in cardiovascular disease progression and regression has been extensively studied in the last two decades. One group of these metabolites is HETE, based on the oxidation reaction's position in the AA structure, these metabolites are divided into the terminal, sub-terminal, and mid-chain HETEs. The terminal (20-HETE) and mid-chain HETEs (8, 9, 11, 12, 14, and 15 HETE) have become the most metabolites explored(Maayah et al., 2017; Roman & Fan, 2018). However, less attention has been paid to subterminal HETEs, including 16-, 17-, 18,- and 19-HETE, despite their unique feature of having two enantiomers: R and S. According to a previous study by Brocks (2006), each enantiomer of chiral compounds will pose distinguished properties regarding their pharmacokinetic profiles such as absorption, distribution, CYP metabolism, and excretion.

Among subterminal HETEs mentioned above, 16-HETE has received less consideration, presumably due to the assumption that the position of its hydroxyl group is far from the carbon terminal of the AA structure, making it less malignant than others. As a terminal HETE, 20-HETE has been acknowledged to have cardiotoxic properties: i.e., the elevation of this cardiotoxic compound was observed in Ang II-induced hypertension and spontaneously hypertensive rats. In contrast to 20-HETE, 19S-HETE has been reported to protect against Ang II-induced cardiac hypertrophy. Nevertheless, the subterminal location of 16-HETE attracts more worrisome since it is the closest to the mid-chain position, which opts to precipitate the formation of cardiotoxic metabolites via CYP1B1 mediated oxidation. Here, we provided strong evidence that 16-HETE enantiomers pose a significant role in the development of cardiac hypertrophy. In addition, 16R-HETE and 16S-HETE increase CYP1B1 at the transcriptional and post-transcriptional levels.

To evaluate the effect of 16-HETE enantiomers on cardiac hypertrophy, RL-14 cells— a cell line that is derived from non-proliferating primary cultures of human fetal ventricular cardiomyocytes was utilized. This cell line was selected due to its propensity to express CYP1B1, as previously reported (Maayah et al., 2014).

Determining the non-toxic concentrations of 16-HETE enantiomers used in the current study is crucial to ensure cellular viability unaffected during and after the treatment. Therefore, an MTT assay was conducted using increasing concentrations of 16-HETE enantiomers. Based on our MTT result (Figure 3.1) and the previous study in human fetal ventricular cardiomyocytes (Maayah & El-Kadi, 2016b), 20 uM of 16-HETE enantiomers were selected for further investigation since it was non-toxic and retained more than 90% of RL-14 cells viability(Shoieb & El-Kadi, 2018). In addition, it is essential to note that the concentration used in the current study is highly relevant to the corresponding human plasma and tissue levels (Fitzgerald, 2001; Tallima & el Ridi, 2018b). For example, AA concentration has been reported to be 13–44 μM in umbilical cord and intervenous space (Benassayag et al., 1997).

A change in the cellular environment plays a significant role in maintaining the expression of two functionally discrete α and ß myosin heavy chain (MHC) isoforms. For instance, in a particular disease state such as cardiac failure and hypertrophy, the relative expression levels of these isoforms opt to be altered the alpha myosin heavy chain (MHC) isoform shifts to its ß isoform during the hypertrophy event (Huang Y, 2001). The accumulation of these MHC isoforms results in a lack of myosin ATPs enzyme activity, thus enervating the cells. In the long run, cardiomyocytes' systolic function and contractile

performance altered, contributing to the significant development of heart failure. Hence, a relative change in the ß/α MHC ratio is a cardinal sign and a reliable predictor of cardiac hypertrophy.

Furthermore, in response to the stress experienced by ventricular cell walls during heart failure development, potent protective natriuretic peptides such as ANP and BNP were released to alleviate them. Hence, an elevation in cellular ANP concentration indicates ventricular stress in clinical settings, whereas an increase in BNP represents heart failure. Taken together, the upregulation of these markers is considered a good indicator of cardiac stress and hypertrophy.

To determine whether 16-HETEs can induce cardiac hypertrophy and modulate hypertrophic markers, several experiments were performed in the human fetal ventricular cardiomyocytes, RL-14. Our results showed that a 24-h incubation of 16-HETE enantiomers with RL-14 significantly increased the relative cell surface area, indicating cellular hypertrophy. Interestingly, albeit both 16-HETE enantiomers could provoke these detrimental effects, the R enantiomer effect was more pronounced than the S-enantiomer.

In the current study we provided the evidence that 20 uM of 16R-HETE and 16S-HETE can induce cardiac hypertrophy markers such as ß/ α MHC ratio and ANP in RL-14 cells. These results are in agreement with previous reports demonstrating that ischemic and dilated cardiomyopathies are associated with the increased level of the β-MHC/ α- MHC ratio(Reiser et al., 2001). Interestingly, the modulation of these hypertrophic markers due to 16R-HETE was more pronounced than the S-enantiomer, explaining the distinguished degree of RL-14 increase in cell surface area after 16_HETE enantiomers exposure.

It is well established that the development of cardiac hypertrophy is strongly correlated with the induction of CYP1B1, which is responsible for forming the highly reactive AA metabolites: mid-chain HETEs (Carrera et al., 2020b; Korashy & El-Kadi, 2005). Therefore, to determine whether the 16-HETE enantiomers alter CYP1B1, we examined the effect of 16-HETE enantiomers on CYP1B1 at transcriptional and post-transcriptional level.

Our results showed that exposure of RL-14 cells with either 20 uM 16R-HETE or 16S-HETE alone could significantly induce CYP1B1 at the transcriptional level. However, pre-treatment RL-14 cells with the Act-D, an RNA polymerase inhibitor, completely abolished the increases in CYP1B1 mRNA mediated by 16-HETE enantiomers. These data indicate that both 16-HETE enantiomers induce de novo RNA synthesis. Furthermore, CYP1B1 mRNA was translated to CYP1B1 protein as evident by increases in CYP1B1 protein after exposure to both enantiomers. Interestingly the R-enantiomer was more pronounced confirming the enantioselective effect of 16-HETE. In agreement with transcriptional and translational levels, 16-HETE enantiomers also significantly increased CYP1B1 catalytic activity. The latter finding indicated the increase in CYP1B1 mRNA and protein was translated into its functional activity. The current study results highlight the first subterminal HETE that can induce CYP1B1. Also, one of the most striking findings of the study is that the capacity of 16R-HETE in causing the CYP1B1 modulation was always more prominent than its enantiomer, 16S-HETE. Taken together, it was evident that the structural orientation affects 16-HETE biological properties.

To confirm the transcriptional effects of both 16-HETE enantiomers, we tested the effect of these subterminal HETEs on XRE-driven luciferase reporter genes that regulate

CYP1B1 transcription. In this study, the luciferase assay was done using human hepatoma HepG2 that has been stably transfected for two reasons: 1) stably transfected cells demonstrate homogenous expression of luciferase reporter genes, and 2) these cells have proven to be a valuable model for investigations of CYP1B1 regulation. Our results demonstrate that both enantiomers of 16-HETE significantly increased the XRE-driven luciferase activity and further strengthen our hypothesis that both 16R-HETE and 16S-HETE upregulate CYP1B1 through a transcriptional mechanism.

To determine whether the modulation of CYP1B1 only transpires at the transcriptional level, we followed up with a subsequent experiment to explore whether a post-transcriptional and a post-translational mechanism are also involved. Through an Act-D and CHX chase experiment in the RL-14 cells, respectively, it is apparent that neither 16R-HETE nor 16S-HETE alters the stability of CYP1B1 mRNA and protein level. These results provide a solid piece of evidence that post-transcriptional and post-translational mechanisms are not involved in the CYP1B1 modulatory outcomes by both 16-HETE enantiomers.

Taken all together, the results presented here provide the first cardinal evidence that both enantiomers of 16-HETE could directly increase the expression of CYP1B1 through a transcriptional mechanism, explaining the mechanism by which 16-HETE enantiomers increases cellular hypertrophy in RL-14 cells.

CYPs enzymes play a prominent role in health and disease conditions, as they are responsible for the metabolism of various endogenous and xenobiotic compounds. Among this superfamily enzyme, the CYP1 family has demonstrated its clinical significance; i.e.,

CYP1B1 has been widely acknowledged to be involved in miscellaneous cardiovascular events (Kaur-Knudsen et al., 2009).

To determine whether 16-HETE enantiomers directly affect CYP1B1 catalytic activity we used in the presence of 7-ER with or without increasing concentrations (0-40 nM) of 16-HETE enantiomers. The O-dealkylation of 7-ethoxyresorufin is a prominent and highly sensitive assay to measure CYP1B1 activity (McFadyen et al., 2004). Interestingly we found that both enantiomers significantly increased the CYP1B1 activity in recombinant human CYP1B1, suggesting allosteric mechanism is involved. To determine whether the increase by 16-HETE enantiomers is unique for CYP1B1, we examined the effect of 16-HETE enantiomers on recombinant human CYP1A2 (which is regulated by the AhR similar to CYP1B1). Therefore. we tested the effect of 10 and 20 nM of 16-HETE enantiomers on MROD activity mediated by recombinant human CYP1A2. Like EROD, MROD (methoxyresorufin O-deoalkylation) assay is a widely available and highly sensitive assay for measuring CYP1A2 activity. Surprisingly, a significant inhibition of CYP1A2 mediated MROD activity was observed with both 16R-HETE and 16S-HETE, and 16R-HETE was pronounced compared to its enantiomer: 16S-HETE. These data confirm the specific effect of 16-HETE enantiomers on CYP1B1.

One of the most peculiar findings in the current study is that the curves of non-linear regression analysis of both experiments are not compatible with the classical Michaelis Menten model; instead, the most probable binding mode fits a sigmoidal (S-shaped) one. It has been widely acknowledged that classical Michaelis Menten portrays that the interaction between the enzyme and substrate occurs in one orthosteric (active) binding site. However, the sigmoidal curve indicated a delay in the reaction rate at the early enzyme-substrate

interaction where a small amount of substrate was available in the environment. However, as more substrates were added to the mixture, the velocity increased exponentially. According to Jansen et al., it occurred because the substrates bind to numerous potential binding sites, characterized by the Hill coefficient.

A Hill coefficient equals 1, which is usually yielded by Michaelis Menten fitted curve, indicates an independent binding in the orthosteric site. However, the hill coefficient greater or lower than one indicates that a substrate or another ligand binds to another probable binding site available in the enzyme body, widely known as allosteric sites. Since 16-HETE co-exposure in the human recombinant CYP1B1 and CYP1A2 with 16-HETE enantiomers produced a sigmoidal fit curve and hill coefficient $\neq 1$, indicating that both CYP1B1 and CYP1A2 have more than one possible binding site.

Generally, the kinetic properties of allosteric enzymes are often explained in terms of a conformational change between a low-activity, low-affinity, or T (tense) state; and a high-activity, high affinity, or R (relaxed) state. Consequent upon an effector binding to an allosteric site, there is a conformational change in the orthosteric site, affecting the enzyme's affinity towards the following substrate molecules: either activation or inhibition. Albeit there is a contradiction in the effect of 16-HETE enantiomers in activities of different CYP1 enzymes, it is evident that both enantiomers of 16-HETE act as an effector on them. While it is an allosteric activator for CYP1B1, it is an allosteric inhibitor for CYP1A2.

In the case of 16-HETE enantiomers modulating CYP1B1 activity, an allosteric activation was involved. Allosteric activation, commonly known as positive allosteric modulation, occurs when an enzyme affinity increases the subsequent ligand binding to the allosteric site. In this scenario, as 16R-HETE or 16S-HETE bound to an allosteric site of

CYP1B1, there was a change in orthosteric site conformation into the R-state, allowing more 7-ER to bind to itincreasing the EROD reaction rate.

Surprisingly enough, as per 16-HETE enantiomers modulating CYP1A2 activity, an allosteric inhibition occurred. In contrast to the previous scenario in CYP1B1, binding of either 16R-HETE or 16S-HETE to the CYP1A2 allosteric site induces a conformational change in its orthosteric site into the T-state, preventing more MR to bind to it; thus, decreasing the resorufin formation rate. On top of that, an increase in 16-HETE enantiomers concentration solidifies these relaxed or tense states and signifies the affinity of these allosteric CYP enzymes intensifying the activity.

In recent years, there has been growing interest in the allostery of CYP. In agreement with our finding, a study by Davidov and Halpert (2012) highlighted that a ligand-induced conformational modification had been recognized to precipitate the typical kinetic behavior of several members of these superfamily enzymes, including CYP2A6, CYP2B4, CYP2B6, CYP2C9, CYP2D6, and CYP3A4. In this regard, CYP3A4 has been widely investigated due to its clinical significance.

By structural homology, CYP enzymes that share more than 40% similarity in the amino acid sequences will be classified under the same family. However, isoenzymes under one family require 55% similarity in amino acids sequence to be classified in the same subfamily. Because CYP1B1 and CYP1A2 only share only 37% resemblance in amino acid sequence, they are assigned in different subfamilies: they. In addition to that, CYP1B1 and CYP1A2 were assigned in one family because they fall under a similar regulation pathway by aryl hydrocarbon receptor (AhR) and have relative substrate specificity.

In reality, both CYP1B1 and CYP1A2 are constituted in human liver microsomes. Therefore, to confirm our findings from the current studies on the recombinant enzyme, we have examined the stimulatory and inhibitory effect of 16-HETE enantiomers on EROD and MROD activity, respectively, mediated by human liver microsomes. In agreement with our finding, a significant increase in EROD reaction rate and a significant decrease in MROD reaction rate was observed, confirming the allostery properties of 16-HETE enantiomers in a plausible scenario in human liver microsomes.

4.2. General Conclusions

Our result shows that 16R-HETE and 16S-HETE, subterminal HETE, significantly increase the cell surface are of human fetal cardiomyocyte, RL-14 cells. They also cause significant induction of hypertrophic marker gene expressions such as ANP, BNP, and B/A MHC ratio, confirming the cellular hypertrophy. Since cardiac hypertrophy is strongly correlated with CYP1B1 expressions, the current study also provides evidence that both enantiomers of 16-HETE upregulate human CYP1B1 at gene, protein, and activity levels in human ventricular myocytes: RL-14 cells. The modulatory properties of the 16R-HETE are apt to be greater than its regioenantiomer, 16S-HETE. In an attempt to understand this phenomenon more profoundly, we demonstrated that the modulation occurred through a transcriptional mechanism. It was apparent that the induced CYP1B1 mRNA was inhibited by an mRNA transcription inhibitor, Act-D. In addition, the luciferase assay confirmed the transcriptional mechanism as 16-HETE enantiomers increase the activity of XRE-driven firefly luciferase. Furthermore, it has been evident that the subterminal HETE did not alter the stability of CYP1B1 mRNA and protein, indicating that there was neither post-

transcriptional nor post-translational modification involved in 16-HETE enantiomers modulated CYP1B1 expressions. In addition, a direct increase in CYP1B1 activity was also observed by human recombinant CYP1B1 and human liver microsomes. Sigmoidal binding mode representing the CYP1B1 activity upon 16-HETE enantiomers demonstrate that the modulation of CYP1B1 activity might occurred through an allosteric mechanism.

4.3. Future Directions

The result of the present work presents a vital modality in which 16-HETE enantiomers could induce CYP1B1 expressions and activity. However, more studies are required to confirm these findings and to further evaluate the modulatory capacity of subterminal HETE:

1. To determine the ability of 16-HETE enantiomers to cause cardiac hypertrophy in in-vivo model.
2. Computational study to assess the allosteric binding of 16-HETE enantiomers on CYP1B1 enzyme by determining the amino acid in the allosteric binding pocket responsible for the structural conformation of CYP1B1 and other CYP enzymes.

References

1-s2.0-S002228368371380X-main. (2012).

REPORT ON THE HEALTH OF CANADIANS. 2016

Aliwarga, T., Evangelista, E. A., Sotoodehnia, N., Lemaitre, R. N., & Totah, R. A. (2018). Regulation of CYP2J2 and EET levels in cardiac disease and diabetes. In *International Journal of Molecular Sciences* (Vol. 19, Issue 7). MDPI AG. https://doi.org/10.3390/ijms19071916

Alsubait, A., Aldossary, W., Rashid, M., Algamdi, A., & Alrfaei, B. M. (2020). CYP1B1 gene: Implications in glaucoma and cancer. In *Journal of Cancer* (Vol. 11, Issue 16, pp. 4652–4661). Ivyspring International Publisher. https://doi.org/10.7150/jca.42669

Anwar-mohamed, A., Zordoky, B. N. M., Aboutabl, M. E., & El-Kadi, A. O. S. (2010). Alteration of cardiac cytochrome P450-mediated arachidonic acid metabolism in response to lipopolysaccharide-induced acute systemic inflammation. *Pharmacological Research*, *61*(5), 410–418. https://doi.org/10.1016/j.phrs.2009.12.015

Bernardo, B. C., Weeks, K. L., Pretorius, L., & McMullen, J. R. (2010a). Molecular distinction between physiological and pathological cardiac hypertrophy: Experimental findings and therapeutic strategies. In *Pharmacology and Therapeutics* (Vol. 128, Issue 1, pp. 191–227). https://doi.org/10.1016/j.pharmthera.2010.04.005

Bernardo, B. C., Weeks, K. L., Pretorius, L., & McMullen, J. R. (2010b). Molecular distinction between physiological and pathological cardiac hypertrophy:

Experimental findings and therapeutic strategies. In *Pharmacology and Therapeutics* (Vol. 128, Issue 1, pp. 191–227). https://doi.org/10.1016/j.pharmthera.2010.04.005

Cabello-Verrugio, C., Vilos, C., Rodrigues-Diez, R., & Estrada, L. (2018). Oxidative stress in disease and aging: Mechanisms and therapies 2018. In *Oxidative Medicine and Cellular Longevity* (Vol. 2018). Hindawi Limited. https://doi.org/10.1155/2018/2835189

Camici, P. G., Tschöpe, C., di Carli, M. F., Rimoldi, O., & van Linthout, S. (2020). Coronary microvascular dysfunction in hypertrophy and heart failure. In *Cardiovascular Research* (Vol. 116, Issue 4, pp. 806–816). Oxford University Press. https://doi.org/10.1093/cvr/cvaa023

Capdevila, J. H., Falck, J. R., & Harris, R. C. (2000). Cytochrome P450 and arachidonic acid bioactivation: molecular and functional properties of the arachidonate monooxygenase Supplementary key words cytochrome P450 • fatty acid hydroxylase • arachidonic acid • eicosanoids • arachidonic acid monooxygenase • arachidonic acid epoxygenase • EET • HETE • salt sensitivity • hyper-tension • hyperpolarizing factor • EDHF. In *Journal of Lipid Research* (Vol. 41).

Capdevila, J. H., Wang, W., & Falck, J. R. (2015). Arachidonic acid monooxygenase: Genetic and biochemical approaches to physiological/pathophysiological relevance. In *Prostaglandins and Other Lipid Mediators* (Vol. 120, pp. 40–49). Elsevier Inc. https://doi.org/10.1016/j.prostaglandins.2015.05.004

Carrera, A. N., Grant, M. K. O., & Zordoky, B. N. (2020a). CYP1B1 as a therapeutic target in cardio-oncology. In *Clinical Science* (Vol. 134, Issue 21, pp. 2897–2927). Portland Press Ltd. https://doi.org/10.1042/CS20200310

Carrera, A. N., Grant, M. K. O., & Zordoky, B. N. (2020b). CYP1B1 as a therapeutic target in cardio-oncology. In *Clinical Science* (Vol. 134, Issue 21, pp. 2897–2927). Portland Press Ltd. https://doi.org/10.1042/CS20200310

Chang, G. W. M., & Kam, P. C. A. (2017). *The physiological and pharmacological roles of cytochrome P450 isoenzymes*.

Cox, M. B., & Miller III, C. A. (2004). Cooperation of heat shock protein 90 and p23 in aryl hydrocarbon receptor signaling. In *Cell Stress & Chaperones* (Vol. 9, Issue 1). Cell Stress Society International.

Dai, C. L., Shi, J., Chen, Y., Iqbal, K., Liu, F., & Gong, C. X. (2013). Inhibition of protein synthesis alters protein degradation through activation of protein kinase B (AKT). *Journal of Biological Chemistry*, *288*(33), 23875–23883. https://doi.org/10.1074/jbc.M112.445148

Dakarapu, R., Errabelli, R., Manthati, V. L., Michael Adebesin, A., Barma, D. K., Barma, D., Garcia, V., Zhang, F., Laniado Schwartzman, M., & Falck, J. R. (2019). 19-Hydroxyeicosatetraenoic acid analogs: Antagonism of 20-hydroxyeicosatetraenoic acid-induced vascular sensitization and hypertension. *Bioorganic and Medicinal Chemistry Letters*, *29*(19). https://doi.org/10.1016/j.bmcl.2019.08.020

de Caterina, R. (2011). n-3 Fatty Acids in Cardiovascular Disease. In *n engl j med* (Vol. 364).

Denisov, I. G., Grinkova, Y. v., Nandigrami, P., Shekhar, M., Tajkhorshid, E., & Sligar, S. G. (2019). Allosteric Interactions in Human Cytochrome P450 CYP3A4: The Role of Phenylalanine 213. *Biochemistry*, *58*(10), 1411–1422. https://doi.org/10.1021/acs.biochem.8b01268

di Cera, E. (2009). Kinetics of allosteric activation. In *Methods in enzymology* (Vol. 466, pp. 259–271). https://doi.org/10.1016/s0076-6879(09)66011-0

Dong, L., Yuan, C., Orlando, B. J., Malkowski, M. G., & Smith, W. L. (2016). Fatty acid binding to the allosteric subunit of cyclooxygenase-2 relieves a tonic inhibition of the catalytic subunit. *Journal of Biological Chemistry*, *291*(49), 25641–25655. https://doi.org/10.1074/jbc.M116.757310

Drazner, M. H. (2011). The progression of hypertensive heart disease. *Circulation*, *123*(3), 327–334. https://doi.org/10.1161/CIRCULATIONAHA.108.845792

Elkhatali, S., Maayah, Z. H., El-Sherbeni, A. A., Elshenawy, O. H., Abdelhamid, G., Shoieb, S. M., & El-Kadi, A. O. S. (2017). *Inhibition of Mid-chain HETEs Protects Against Angiotensin II-induced Cardiac Hypertrophy*. www.jcvp.org

Fitzgerald, G. A. (2001). PERSPECTIVE SERIES Prostaglandins and their precursors. In *The Journal of Clinical Investigation* (Vol. 107, Issue 11).

Franchina, D. G., Dostert, C., & Brenner, D. (2018). Reactive Oxygen Species: Involvement in T Cell Signaling and Metabolism. In *Trends in Immunology* (Vol. 39, Issue 6, pp. 489–502). Elsevier Ltd. https://doi.org/10.1016/j.it.2018.01.005

Frey, N., & Olson, E. N. (2003). Cardiac Hypertrophy: The Good, the Bad, and the Ugly. In *Annual Review of Physiology* (Vol. 65, pp. 45–79). https://doi.org/10.1146/annurev.physiol.65.092101.142243

Gui, Y., Chen, J., Hu, J., Liao, C., Ouyang, M., Deng, L., Yang, J., & Xu, D. (2020). Soluble epoxide hydrolase inhibitors improve angiogenic function of endothelial progenitor cells via ERK/p38-mediated miR-126 upregulation in myocardial infarction mice

after exercise. *Experimental Cell Research*, *397*(2). https://doi.org/10.1016/j.yexcr.2020.112360

Haidar, R., Henkler, F., Kugler, J., Rosin, A., Genkinger, D., Laux, P., & Luch, A. (2021). The role of DNA-binding and ARNT dimerization on the nucleo-cytoplasmic translocation of the aryl hydrocarbon receptor. *Scientific Reports*, *11*(1). https://doi.org/10.1038/s41598-021-97507-w

Hanna, V. S., & Hafez, E. A. A. (2018). Synopsis of arachidonic acid metabolism: A review. In *Journal of Advanced Research* (Vol. 11, pp. 23–32). Elsevier B.V. https://doi.org/10.1016/j.jare.2018.03.005

Jacob, A., Hartz, A. M. S., Potin, S., Coumoul, X., Yousif, S., Scherrmann, J. M., Bauer, B., & Declèves, X. (2011). Aryl hydrocarbon receptor-dependent upregulation of Cyp1b1 by TCDD and diesel exhaust particles in rat brain microvessels. *Fluids and Barriers of the CNS*, *8*(1). https://doi.org/10.1186/2045-8118-8-23

Kapelyukh, Y., Henderson, C. J., Scheer, N., Rode, A., & Wolf, C. R. (2019). Defining the contribution of CYP1A1 and CYP1A2 to drug metabolism using humanized CYP1A1/1A2 and Cyp1a1/Cyp1a2 knockout mice. *Drug Metabolism and Disposition*, *47*(8), 907–918. https://doi.org/10.1124/dmd.119.087718

Kaur-Knudsen, D., Nordestgaard, B. G., Tybjaerg-Hansen, A., & Bojesen, S. E. (2009). CYP1B1 genotype and risk of cardiovascular disease, pulmonary disease, and cancer in 50000 individuals. *Pharmacogenetics and Genomics*, *19*(9), 685–694. https://doi.org/10.1097/FPC.0b013e32833042cb

Korashy, H. M., el Gendy, M. A. M., Alhaider, A. A., & El-Kadi, A. O. (2012). Camel milk modulates the expression of aryl hydrocarbon receptor-regulated genes, Cyp1a1,

Nqo1, and Gsta1, in murine hepatoma hepa 1c1c7 cells. *Journal of Biomedicine and Biotechnology*, *2012*. https://doi.org/10.1155/2012/782642

Korashy, H. M., & El-Kadi, A. O. S. (2005). Regulatory mechanisms modulating the expression of cytochrome P450 1A1 gene by heavy metals. *Toxicological Sciences*, *88*(1), 39–51. https://doi.org/10.1093/toxsci/kfi282

Kors, S. (2019). Regulation of Proteasome Activity by (Post-)transcriptional Mechanisms. In *Frontiers in Molecular Biosciences* (Vol. 6). Frontiers Media S.A. https://doi.org/10.3389/fmolb.2019.00048

Kotaka, M., Ren, J., Lockyer, M., Hawkins, A. R., & Stammers, D. K. (2006). Structures of R- and T-state Escherichia coli aspartokinase III: Mechanisms of the allosteric transition and inhibition by lysine. *Journal of Biological Chemistry*, *281*(42), 31544–31552. https://doi.org/10.1074/jbc.M605886200

Kumar, A., Behl, T., Jamwal, S., Kaur, I., Sood, A., & Kumar, P. (2020). Exploring the molecular approach of COX and LOX in Alzheimer's and Parkinson's disorder. In *Molecular Biology Reports* (Vol. 47, Issue 12, pp. 9895–9912). Springer Science and Business Media B.V. https://doi.org/10.1007/s11033-020-06033-x

Letter to the Editor CONSTITUTIVE AND INDUCIBLE EXPRESSION OF CYTOCHROME P450IA1 AND P450IB1 IN HUMAN VASCULAR ENDOTHELIAL AND SMOOTH MUSCLE CELLS. (1998).

Li, F., Zhu, W., & Gonzalez, F. J. (2017). Potential role of CYP1B1 in the development and treatment of metabolic diseases. In *Pharmacology and Therapeutics* (Vol. 178, pp. 18–30). Elsevier Inc. https://doi.org/10.1016/j.pharmthera.2017.03.007

Liu, W. jun, Wang, T., Wang, B., Liu, X. tian, He, X. wei, Liu, Y. jian, Li, Z. xi, Tan, R., & Zeng, H. song. (2015). CYP2C8-derived epoxyeicosatrienoic acids decrease oxidative stress-induced endothelial apoptosis in development of atherosclerosis: Role of Nrf2 activation. *Journal of Huazhong University of Science and Technology - Medical Science*, *35*(5), 640–645. https://doi.org/10.1007/s11596-015-1483-5

Liu, X., Davis, C. M., & Alkayed, N. J. (2018). P450 eicosanoids and reactive oxygen species interplay in brain injury and neuroprotection. In *Antioxidants and Redox Signaling* (Vol. 28, Issue 10, pp. 987–1007). Mary Ann Liebert Inc. https://doi.org/10.1089/ars.2017.7056

Lowe Furge, L., & Guengerich, F. P. (2006). *Mini-Series: Modern Metabolic Concepts Cytochrome P450 Enzymes in Drug Metabolism and Chemical Toxicology AN INTRODUCTION*. www.issx.org/

Lucas, D., Goulitquer, S., Marienhagen, J., Fer, M., Dreano, Y., Schwaneberg, U., Amet, Y., & Corcos, L. (2010). Stereoselective epoxidation of the last double bond of polyunsaturated fatty acids by human cytochromes P450. *Journal of Lipid Research*, *51*(5), 1125–1133. https://doi.org/10.1194/jlr.M003061

Ma YH, Harder DR, Clark JE, Roman RJ. Effects of 12-HETE on isolated dog renal arcuate arteries. Am J Physiol. 1991 Aug;261(2 Pt 2):H451-6. doi: 10.1152/ajpheart.1991.261.2.H451. PMID: 1908641.

Maayah, Z. H., Althurwi, H. N., El-Sherbeni, A. A., Abdelhamid, G., Siraki, A. G., & El-Kadi, A. O. S. (2017). The role of cytochrome P450 1B1 and its associated mid-chain hydroxyeicosatetraenoic acid metabolites in the development of cardiac

hypertrophy induced by isoproterenol. *Molecular and Cellular Biochemistry*, *429*(1–2), 151–165. https://doi.org/10.1007/s11010-017-2943-y

Maayah, Z.H., & Elshenawy, Osama & Althurwi, Hassan & Abdelhamid, Ghada & El-Kadi, Ayman. (2014). Human fetal ventricular cardiomyocyte, RL-14 cell line, is a promising model to study drug metabolizing enzymes and their associated arachidonic acid metabolites. Journal of Pharmacological and Toxicological Methods. 71. 10.1016/j.vascn.2014.11.005.

Maayah, Z. H., & El-Kadi, A. O. S. (2016a). The role of mid-chain hydroxyeicosatetraenoic acids in the pathogenesis of hypertension and cardiac hypertrophy. In *Archives of Toxicology* (Vol. 90, Issue 1, pp. 119–136). Springer Verlag. https://doi.org/10.1007/s00204-015-1620-8

Maayah, Z. H., & El-Kadi, A. O. S. (2016b). 5-, 12- and 15-Hydroxyeicosatetraenoic acids induce cellular hypertrophy in the human ventricular cardiomyocyte, RL-14 cell line, through MAPK- and NF-κB-dependent mechanism. *Archives of Toxicology*, *90*(2), 359–373. https://doi.org/10.1007/s00204-014-1419-z

McFadyen, M. C. E., Melvin, W. T., & Murray, G. I. (2004). Cytochrome P450 CYP1B1 activity in renal cell carcinoma. *British Journal of Cancer*, *91*(5), 966–971. https://doi.org/10.1038/sj.bjc.6602053

Nannelli, A., Rossignolo, F., Tolando, R., Rossato, P., Longo, V., & Gervasi, P. G. (2009). Effect of β-naphthoflavone on AhR-regulated genes (CYP1A1, 1A2, 1B1, 2S1, Nrf2, and GST) and antioxidant enzymes in various brain regions of pig. *Toxicology*, *265*(3), 69–79. https://doi.org/10.1016/j.tox.2009.09.010

Nebert, D. W. (2017). Aryl hydrocarbon receptor (AHR): "pioneer member" of the basic-helix/loop/helix per-Arnt-sim (bHLH/PAS) family of "sensors" of foreign and endogenous signals. In *Progress in Lipid Research* (Vol. 67, pp. 38–57). Elsevier Ltd. https://doi.org/10.1016/j.plipres.2017.06.001

Ni, K. di, & Liu, J. Y. (2021). The Functions of Cytochrome P450 ω-hydroxylases and the Associated Eicosanoids in Inflammation-Related Diseases. In *Frontiers in Pharmacology* (Vol. 12). Frontiers Media S.A. https://doi.org/10.3389/fphar.2021.716801

Nishimura, M., & Naito, S. (n.d.). *Tissue-speci˜c mRNA Expression Pro˜les of Human ATP-binding Cassette and Solute Carrier Transporter Superfamilies*. http://www.jstage.jst.go.jp/browse/dmpk

Pappas, B., Yang, Y., Wang, Y., Kim, K., Chung, H. J., Cheung, M., Ngo, K., Shinn, A., & Chan, W. K. (2018). p23 protects the human aryl hydrocarbon receptor from degradation via a heat shock protein 90-independent mechanism. *Biochemical Pharmacology*, *152*, 34–44. https://doi.org/10.1016/j.bcp.2018.03.015

Polic, V., & Auclair, K. (2017.). *Allosteric Activation of Cytochrome P450 3A4 via Progesterone Bioconjugation*.

Polic, V., Sevrioukova, I. F., & Auclair, K. (2018). Steroid bioconjugation to a CYP3A4 allosteric site and its effect on substrate binding and coupling efficiency. *Archives of Biochemistry and Biophysics*, *653*, 90–96. https://doi.org/10.1016/j.abb.2018.06.014

Pregnancy-induced physiological heart hypertrophy. (n.d.). www.AJCD.us

Rahman, M., Wright, J. T., & Douglas, J. G. (1997). The Role of the Cytochrome P450-Dependent Metabolites of Arachidonic Acid in Blood Pressure Regulation and Renal

Function A Review. In *AJH* (Vol. 10). https://academic.oup.com/ajh/article/10/3/356/213848

Ramazi, S., & Zahiri, J. (2021). Post-translational modifications in proteins: Resources, tools and prediction methods. In *Database* (Vol. 2021). Oxford University Press. https://doi.org/10.1093/database/baab012

Rezende, F., Prior, K. K., Löwe, O., Wittig, I., Strecker, V., Moll, F., Helfinger, V., Schnütgen, F., Kurrle, N., Wempe, F., Walter, M., Zukunft, S., Luck, B., Fleming, I., Weissmann, N., Brandes, R. P., & Schröder, K. (2017). Cytochrome P450 enzymes but not NADPH oxidases are the source of the NADPH-dependent lucigenin chemiluminescence in membrane assays. *Free Radical Biology and Medicine*, *102*, 57–66. https://doi.org/10.1016/j.freeradbiomed.2016.11.01

Robinson, P. K. (2015). Enzymes: principles and biotechnological applications. *Essays in Biochemistry*, *59*, 1–41. https://doi.org/10.1042/BSE0590001

Rocic, P., & Schwartzman, M. L. (2018). 20-HETE in the regulation of vascular and cardiac function. *Pharmacology & therapeutics*, *192*, 74–87. https://doi.org/10.1016/j.pharmthera.2018.07.004

Roman, R. J., & Fan, F. (2018). 20-HETE: Hypertension and beyond. *Hypertension*, *72*(1), 12–18. https://doi.org/10.1161/HYPERTENSIONAHA.118.10269

Rothman, S. (2010). How is the balance between protein synthesis and degradation achieved? *Theoretical Biology and Medical Modelling*, *7*(1). https://doi.org/10.1186/1742-4682-7-25

Samokhvalov, V., Jamieson, K. L., Darwesh, A. M., Keshavarz-Bahaghighat, H., Lee, T. Y. T., Edin, M., Lih, F., Zeldin, D. C., & Seubert, S. J. M. (2019). Deficiency of soluble

epoxide hydrolase protects cardiac function impaired by LPS-induced acute inflammation. *Frontiers in Pharmacology*, *9*(JAN). https://doi.org/10.3389/fphar.2018.01572

Satsu, H., Yoshida, K., Mikubo, A., Ogiwara, H., Inakuma, T., & Shimizu, M. (2015). Establishment of a stable aryl hydrocarbon receptor-responsive HepG2 cell line. *Cytotechnology*, *67*(4), 621–632. https://doi.org/10.1007/s10616-014-9711-6

Shimizu, I., & Minamino, T. (2016). Physiological and pathological cardiac hypertrophy. In *Journal of Molecular and Cellular Cardiology* (Vol. 97, pp. 245–262). Academic Press. https://doi.org/10.1016/j.yjmcc.2016.06.001

Shoieb, S. M., & El-Kadi, A. O. S. (2018). S-enantiomer of 19-hydroxyeicosatetraenoic acid preferentially protects against angiotensin II-induced cardiac hypertrophy. *Drug Metabolism and Disposition*, *46*(8), 1157–1168. https://doi.org/10.1124/dmd.118.082073

Shoieb, S. M., & El-Kadi, A. O. S. (2020). Resveratrol attenuates angiotensin II-induced cellular hypertrophy through the inhibition of CYP1B1 and the cardiotoxic mid-chain HETE metabolites. *Molecular and Cellular Biochemistry*, *471*(1–2), 165–176. https://doi.org/10.1007/s11010-020-03777-9

Smale, S. T. (2010). Luciferase assay. *Cold Spring Harbor Protocols*, *5*(5). https://doi.org/10.1101/pdb.prot5421

Sokoła-Wysoczańska, E., Wysoczański, T., Wagner, J., Czyż, K., Bodkowski, R., Lochyński, S., & Patkowska-Sokoła, B. (2018). Polyunsaturated fatty acids and their potential therapeutic role in cardiovascular system disorders—a review. In *Nutrients* (Vol. 10, Issue 10). MDPI AG. https://doi.org/10.3390/nu10101561

Spector, A. A. (2009a). Arachidonic acid cytochrome P450 epoxygenase pathway. In *Journal of Lipid Research* (Vol. 50, Issue SUPPL.). https://doi.org/10.1194/jlr.R800038-JLR200

Spector, A. A. (2009b). Arachidonic acid cytochrome P450 epoxygenase pathway. In *Journal of Lipid Research* (Vol. 50, Issue SUPPL.). https://doi.org/10.1194/jlr.R800038-JLR200

Spector, A. A., & Norris, A. W. (2007). Action of epoxyeicosatrienoic acids on cellular function. *Am J Physiol Cell Physiol*, *292*, 996–1012. https://doi.org/10.1152/ajpcell.00402.2006.-Epoxyeicosatrienoic

Stroumpoulis, K. I. (2010). Hypertrophic cardiomyopathy and sudden cardiac death. *World Journal of Cardiology*, *2*(9), 289. https://doi.org/10.4330/wjc.v2.i9.289

Sugase, K., Landes, M. A., Wright, P. E., & Martinez-Yamout, M. (2008.). *Overexpression of post-translationally modified peptides in Escherichia coli by co-expression with modifying enzymes*.

Tallima, H., & el Ridi, R. (2018a). Arachidonic acid: Physiological roles and potential health benefits – A review. In *Journal of Advanced Research* (Vol. 11, pp. 33–41). Elsevier B.V. https://doi.org/10.1016/j.jare.2017.11.004

Tallima, H., & el Ridi, R. (2018b). Arachidonic acid: Physiological roles and potential health benefits – A review. In *Journal of Advanced Research* (Vol. 11, pp. 33–41). Elsevier B.V. https://doi.org/10.1016/j.jare.2017.11.004

Waldman, M., Peterson, S. J., Arad, M., & Hochhauser, E. (2016). The role of 20-HETE in cardiovascular diseases and its risk factors. In *Prostaglandins and Other Lipid*

Mediators (Vol. 125, pp. 108–117). Elsevier Inc. https://doi.org/10.1016/j.prostaglandins.2016.05.007

Westphal, C., Konkel, A., & Schunck, W. H. (2015). Cytochrome P450 enzymes in the bioactivation of polyunsaturated fatty acids and their role in cardiovascular disease. *Advances in Experimental Medicine and Biology*, *851*, 151–187. https://doi.org/10.1007/978-3-319-16009-2_6

Yang, T., Peng, R., Guo, Y., Shen, L., Zhao, S., & Xu, D. (2013). The role of 14,15-dihydroxyeicosatrienoic acid levels in inflammation and its relationship to lipoproteins. *Lipids in Health and Disease*, *12*. https://doi.org/10.1186/1476-511X-12-151